A novel biomass gasification micro-cogeneration plant: experimental and numerical analysis

Cirillo, D.
CMD S.p.A., Research & Development Department, Via Pacinotti, 2, 81020 S. Nicola La Strada (Caserta), Italy
domenico.cirillo@cmdengine.com

Di Palma, M.
Department of Engineering, University of Naples "Parthenope", Centro Direzionale, Isola C4, 80143 Naples, Italy
maria.dipalma@uniparthenope.it

La Villetta, M.
CMD S.p.A., Research & Development Department, Via Pacinotti, 2, 81020 S. Nicola La Strada (Caserta), Italy
maurizio.lavilletta@cmdengine.com

Macaluso, A.
Department of Engineering, University of Naples "Parthenope", Centro Direzionale, Isola C4, 80143 Naples, Naples, Italy
adriano.macaluso@uniparthenope.it

Mauro, A.
Department of Engineering, University of Naples "Parthenope", Centro Direzionale, Isola C4, 80143 Naples, Naples, Italy
alessandro.mauro@uniparthenope.it

Vanoli, L. *
Department of Engineering, University of Naples "Parthenope", Centro Direzionale, Isola C4, 80143 Naples, Naples, Italy
laura.vanoli@uniparthenope.it

*Corresponding.

Abstract

This work presents a numerical model developed to predict the behaviour of a real micro-cogeneration biomass gasification system, based on a fixed-bed downdraft gasifier, coupled with a spark-ignition internal combustion engine. The model developed by the authors takes into account all the thermo-physical processes occurring in the whole system: gasification, cleaning, combustion and heat recovery. The numerical model is based on the Gibbs free energy minimization, applying the restricted equilibrium method. The model has been validated with the experimental data collected during an extensive experimental campaign, and a good agreement between measured data and predicted results is obtained. The present validated model has proved to be a useful tool for analyzing the performance of real micro-CHP plants. The global electrical and thermal efficiencies predicted by the model are 19.9% and 17.8%, while the measured values are 19.5% and 21.7%, respectively. Some parametric analyses have been carried out in order to assess the performance of the system as a function of the main gasifier and engine parameters, and to predict the behaviour of the system.

Highlights

A numerical model is developed to predict the behaviour of a real micro-cogeneration system.

The model includes a downdraft gasifier coupled with an internal combustion engine.

The model takes into account gasification, cleaning, combustion and heat recovery.

The numerical model has been validated with the experimental data acquired on site.

The experimental data have been associated to their measurement uncertainties.

Keywords:

Combined Heat and Power; Experimental; Biomass; Gasification; Numerical model; validation.

Nomenclature

Parameters

c_p	water specific heat	kJ/(kg K)
$\dot{E}$	primary power	kW
HHV	higher heating value	MJ/kg
LHV	lower heating value	MJ/kg
$\dot{m}$	mass flow rate	kg/s
m	mass	kg
$\dot{P}$	electric power	kW
p	pressure	bar
$\dot{Q}$	thermal power	kW
T	temperature	°C

t	time	s
y	mass percentage	%

Acronyms, abbreviations

A	mass percentage of ash on dry basis
ANN	artificial neural network
BFB	bubbling fluidized bed
BTDC	before top dead centre
CFB	circulating fluidized bed
CFD	computational fluid dynamics
CGE	cold gas efficiency
CHP	combined heat and power
CMD	Costruzioni Motori Diesel company
DTU	technical University of Denmark
ECO20	ECO20 system
EDR	exchanger design & rating
EFB	empty fruit bunch
ER	equivalence ratio
FICFB	fast internal circulating fluidized bed
ICE	internal combustion engine
k	coverage factor
max	maximum value
MC	biomass moisture content
m-CHP	micro-CHP
n	number of detection
PHE	plate heat exchanger
RDF	refuse derived fuel
RES	renewable energy sources
r.v.	read value
STHE	shell & tube heat exchanger
U	expanded uncertainty
u	uncertainty
W	water content
WHR	Waste Heat Recovery
X	independent/measured variable
x	actual value of the of the independent/measured variable
Y	dependent variable
y	actual value of the of the dependent/calculated variable

Chemical formula

C	mass percentage of carbon on dry basis
CH_4	volume percentage of methane in the syngas
CO	volume percentage of carbon monoxide in the syngas
CO_2	volume percentage of carbon dioxide in the syngas
H	mass percentage of hydrogen on dry basis
H_2	volume percentage of hydrogen in the syngas
H_2O	volume percentage of water in the syngas
N	mass percentage of nitrogen on dry basis

N_2	volume percentage of nitrogen in the syngas
O	mass percentage of oxygen on dry basis
O_2	volume percentage of oxygen in the syngas
S	mass percentage of sulphur on dry basis

Greek letters

α	air-fuel ratio
λ	stoichiometric ratio
η	efficiency
ΔT	difference of Temperature
Δt	period of time

Subscripts

A	A type uncertainty
a1	air entering the reactor
a2	air entering the ICE
ar	as received
B	B type uncertainty
b	biomass
cool	cooling
comb	combustion
dry	on dry basis
el	electric, electricity
ex	exhaust gases
ex1	exhaust gases exiting the ICE
ex2	exhaust gases entering the STHE
ex3	exhaust gases exiting the STHE
g	gasifier
g,exit	syngas exit
i	i-th variable
j	j-th variable
p	primary circuit water
p1	primary circuit water entering the ICE
p2	primary circuit water entering the PHE
p3	primary circuit water entering the ICE Radiator
pyr	pyrolisis
red	reduction
s	secondary circuit water
s1	secondary circuit water entering the PHE
s2	secondary circuit water entering the STHE
s3	secondary circuit water exiting the STHE
st	stoichiometric
syn	syngas
syn1	syngas entering the cyclone
syn2	syngas entering the cooler
syn3	syngas entering the filter
syn4	syngas entering the ICE
SYST	whole system

th	thermal
tot	total

1. Introduction

The depletion of fossil fuel reserves and the Earth's climate changes are serious problems that involve the society nowadays. Among the causes of environmental problems, the combustion of fossil fuels is the major contributor. Many international agreements have been promoted to reduce greenhouse gas emissions using renewable and sustainable energy resources. The European Council has adopted the "2030 Climate and Energy Framework" [1] that sets three key targets to 2030: reducing greenhouse gas emissions by 40.0% from 1990 levels, at least 32.0% of renewable energy sources and an improvement of 32.5% in energy efficiency. The Conference of the Parties COP25, held in Madrid in December 2019, aimed at finalizing the Paris Agreement, to limit the increase in global temperature to 1.50°C.

Renewable Energy Sources (RES) represent a reliable alternative to conventional fossil fuel utilization for their minimal impacts on the environment. RES, such as solar and wind, have the great limit of being intermittent and strongly dependent upon weather conditions, meaning that their dispatch cannot always be assured on demand. Conversely, biomass, hydro and geothermal energy can be stored and continuously used to have a predictable output not dependent on weather conditions [2].

Among all the RES, biomass is a promising option to be used for heat and power production for its flexibility, to be converted to several forms of energy; in fact, biomass is the only renewable source that can be used in solid, liquid or gaseous form [3]. Biomass is mostly referred to plant sources, such as wood from natural forests, waste from agricultural, food waste, industrial waste and sewage sludge. The energy obtained from biomass is a form of renewable energy and it does not add carbon dioxide (CO_2) to the environment [4].

The biomass conversion technologies can be divided into three basic categories: biological conversion, chemical conversion and thermochemical conversion. Generally, the thermochemical conversion of biomass, which can be divided into pyrolysis, gasification and combustion, is more efficient than the other technologies, due to its short reaction time and high conversion efficiency. Gasification is one of the most advanced thermochemical processes to convert biomass into fuel. Biomass gasification is a clean technology allowing the removal of particulates and heavy hydrocarbons compared to combustion or pyrolysis. The gasification process has several advantages, among which its versatility and flexibility to be combined with different secondary conversion technologies and the possibility of using biomass fuels at a wider range of moisture content.

The gaseous mixture produced from biomass gasification, the syngas, mainly contains carbon monoxide (CO), hydrogen (H_2), CO_2 , and methane (CH_4), when gasifying agents (air or oxygen, steam, or CO_2) and temperature larger than 700 °C are considered [5]. Gasification includes drying, pyrolysis, oxidation, reduction, or gasification reactions. The efficiency of conversion depends on biomass material, particle size, gas flow rate, and design of the gasifier.

1.1. Literature overview

Researchers have recorded three principal types of gasifiers, which include fluidized bed gasifiers [6], entrained flow gasifiers [7] and fixed bed gasifiers [8].

Fixed bed gasifiers can be categorized on the direction of gas flow as updraft, downdraft and cross-draft. The downdraft gasifier is the most used for solid biomass, for its appropriate conversion efficiency, lower production of tar and particulate matter [9] and more suitable for small-scale applications [10].

Several experimental studies on biomass gasification have been carried out in the past. Di Blasi et al. [11] designed a laboratory-scale fixed-bed gasification plant to compare the gasification characteristics of several biomass materials, such as beechwood, nutshells, olive husks, and grape residues. Zainal et al. [12] performed an experimental study on a downdraft biomass gasifier using wood chips, and the effects of equivalence ratio (ER) on the gas composition, calorific value and the gas production rate were reported. Dogru et al. [13] carried out gasification studies using hazelnut shells as biomass, a full mass balance was reported, including the tar production rate and the composition of the produced gas as a function of feed rate.

Other authors performed experimental studies using biomass downdraft gasifiers to investigate the parameters influencing the gasification process. Jayah et al. [14] studied a downdraft biomass gasifier using rubberwood as biomass under various conditions and the factors influencing the conversion efficiency were investigated. Hanaoka et al. [15] investigated the role of the three main constituents of woody biomass (cellulose, xylan, and lignin) during gasification using a downdraft fixed bed gasifier. Sheth and Babu [16] carried out experiments using a downdraft biomass gasifier with the waste generated while making furniture. Sharma et al. [17] carried out an experimental study on a 75 kW_{th} downdraft (biomass) gasifier system to determine temperature profile, gas composition, calorific value, and trends for pressure drop across the system. Martínez et al. [18] used a downdraft gasifier with two-air supply stages to reduce the tar content.

The approaches for mathematical modeling of the gasification process are classified into thermodynamic equilibrium, kinetic, phenomenological, and Artificial Neural Network (ANN) models. Thermodynamic equilibrium models are the simplest ones; such models allow predicting the composition of produced syngas, assuming the reactions reach the equilibrium. These models are independent of the gasifier design and can be used to analyze the influence of fuel and process parameters. The equilibrium model may be described by equilibrium constants (stoichiometric method) and minimization of the Gibbs free energy (non-stoichiometric method). Equilibrium models have been used successfully by many researchers [19]–[21] that proposed an equilibrium model for a downdraft gasifier to predict the product gas composition and its calorific value. Vaezi et al. [22] developed a thermodynamic equilibrium model to investigate the effect of the use of oxygen enrichment in the improvement of gas quality. The authors have reported the range of variation of oxygen content for 55 different biomass materials. Barman et al. [23] presented a model for fixed-bed downdraft biomass gasifiers incorporating tar in the global gasification reaction. Silva and Rouboa [24] presented an equilibrium model that considered both homogeneous and heterogeneous equilibrium. Costa et al. [25] considered char produced and added Boudouard reaction and tar produced as a function of the gasification temperature.

The inadequacy of the equilibrium models to correlate the reactor design parameter with the final product gas composition led to the development of kinetic models. Some authors developed kinetic models, considering the kinetics of gasification reactions; these models are more accurate and detailed but computationally intensive. Di Blasi [26] proposed a one-dimensional unsteady-state model for biomass gasification in a stratified downdraft gasifier.

The effect of various parameters, such as the physicochemical properties of feedstock, the plant size, single-particle effects, and char reactivity on the product gas compositions, was discussed. Giltrap et al. [27] proposed a steady-state kinetic model for predicting the product gas composition and temperature inside a downdraft biomass gasifier using the reaction kinetics

parameters. Jayah et al. [14] proposed a kinetic model that consists of two sub-models: pyrolysis and gasification zones. Gordillo and Belghit [28] developed a numerical model of a solar downdraft gasifier of biochar with steam, based on the kinetics model. Tinaut et al. [29] developed a one-dimensional steady-state model for the gasification process in a fixed-bed downdraft biomass gasifier. The model takes into account almost all the phenomena that occur during the gasification process.

The different mass and energy interchanges between the gaseous phase, the solid phase and the reactor wall are considered in the model development. Sharma [30] developed a 1-dimensional steady-state kinetic model to predict the performance of a downdraft biomass gasifier. Five separate zones described the thermochemical processes: preheating zone, drying, pyrolysis, combustion and reduction. Simone et al. [31] proposed a mathematical model, based on the literature kinetic, mass transfer and heat transfer sub-models. The model treats the gas and the solid phase separately and the two phases are correlated by mass and energy fluxes.

The gasification process includes a set of phenomena, such as fluid flow, heat transfer, and complex chemistry, that can be solved by applying governing mathematical equations, mostly based on the conservation laws of mass, heat, and momentum. Computational Fluid Dynamics (CFD) models constitute a valid option for gasification modeling, providing relevant information on temperature and species concentration along the reactor. Gao et al. [32] used an Euler-Lagrange approach, applying a standard k-epsilon model to the continuous and discrete phases for the biomass particle model. Jakobs et al.[33] developed a CFD model of high pressure, entrained flow gasifier. Janajreh et al. [34] investigated the conversion efficiency in a small-scale biomass gasification unit using CFD to model the Lagrangian particle coupled evolution.

ANN models refer to the system's ability to learn from previous experiences and improving the following outputs, mimicking some human features. Some authors used this approach to study biomass gasification. Arnavat et al. [35] developed two ANN models for circulating fluidized bed gasifiers (CFB) and for bubbling fluidized bed gasifiers (BFB), in order to determine the producer gas composition and gas yield. Li et al.[36] developed an ANN model to simulate the influence of two important hydrodynamic factors, heating rate and gasifier length, on hydrogen yield and hydrogen efficiency. Xiao et al. [37] investigated five types of organic components and, based on the experimental data, developed an ANN model to predict gasification characteristics.

Aspen Plus software has been used in the literature to model gasifier systems and assess the performance of the overall process of gasification. Mansaray et al. [38] developed and analyzed a model for gasification of rice husks using a fluidized-bed gasifier. Ramzan et al. [39] developed a steady gasification model of three different biomass feedstocks, i.e. food waste, municipal solid waste, and poultry waste. The simulation model was validated with the experimental data obtained by the authors from the gasification of three wastes in a lab-scale hybrid gasifier. They have observed that the model results were in good agreement with the experimental results. Kuo et al. [40] developed an Aspen Plus-based model to evaluate the gasification potentials of raw bamboo using thermodynamic analysis. Gu et al.[41] developed a model in Aspen Plus of biomass gasification with different gasifying agents. Tavares et al. [42] implemented a model in Aspen Plus for Portuguese forest residues downdraft gasification and performed a sensibility analysis.

The syngas produced by biomass gasification can be used in gas engines, turbines, or fuel cells for Combined Heat and Power (CHP) production with an overall efficiency range between 60% and 90% with a reduction of the global CO_2 emissions. Internal combustion engines (ICEs) are best suited for small and medium-scale plants from 1 to 10 MW. Besides, the advantages of ICEs include low cost, reliability, high operating efficiency, and flexibility. Many large-scale biomass-based power generation plants have been built in the world. However, it is more

feasible to utilize biomass energy directly in the biomass production areas such as villages and rural areas with abundant biomass resources. Therefore, the small-scale gasification power plants (<200 kW_{el}) can be fully used.

China has an enormous amount of biomass resources utilized in small-size rice husk gasification plants [40]. The biomass-based power plants in the U.S.A. have a total capacity of 23 MW; only two of them have a capacity below 1.00 MW: one is in Tennessee and one in New Hampshire with a capacity of 125 kW and 40 kW respectively [43]. In Cuba there are two plants founded by UNIDO, one located in La Melvis with an installed power in the range of 0.50–2.00 MW and one in Cocodrillo of 50 kW [44]. Biomass gasification technology has a fairly good development in the European region. In Denmark, the company Martezo developed a 135 kW_{el} downdraft biomass gasifier at Hølgild, [45]. In Germany, Bio-Heizstoffwerk Berlin GmbH provided biomass gasifiers of 10 - 500 kW_{el}, Wamsler Umwelttechnik GmbH provided a large-scale plant from 600 kW to 11.0 MW. A two-stage 75 kW gasifier named "Viking" was developed by the Technical University of Denmark (DTU) using the woodchip as feedstock. The CHP plant in Güssing (Austria) [46] is a Fast Internal Circulating Fluidized Bed (FICFB) steam gasifier that converts wood chips to a product gas with a heating value of approximately 12.0 MJ/Nm^3 (dry basis). A gasification unit for decentralized CHP production in Greece is designed and built within the framework of the SMARt-CHP LIFE+ project [47]. In Italy, about biomass gasification power plants had been installed by 2018 with a total capacity of over 43.5 MW_{el}, 83.0% of the power plants have capacities between 20 and 200 kW_{el} and supply about 47.0% of the total power [48].

Numerical modeling can be an effective tool to evaluate thermal power plant performance in different operating conditions, providing accurate results regarding plant operations. Baratieri et al. [49] built a model of a biomass gasification unit coupled with ICE, in which syngas production was modelled through a thermodynamic equilibrium approach. Trninic et al. [50] presented a mathematical model of a small-scale CHP system, based on biomass waste downdraft gasification and ICE, powered by corn cobs (as a form of waste biomass) using EES software. Inayat et al. [51] developed a model for a heat integrated plant designed for hydrogen production from oil palm empty fruit bunch (EFB) using MATLAB.

Several authors modelled and simulated CHP systems based on gasification with Aspen Plus software. Villarini et al.[52] presented a paper where an ICE gasification system was simulated and carried out a sensitivity analysis, paying attention to the cold gas efficiency and the Lower Heating Value (LHV) of syngas. Násner et al. [53] developed a model for a Refuse Derived Fuel (RDF) gasification pilot plant using air as a gasification agent integrated with an Otto cycle ICE. Formica et al. [54] developed a model of a full-scale woody biomass gasification plant with a fixed-bed downdraft gasifier, including the technical characteristics of all the components of the plant. Moreover, Emun et al. [55] and Madzivhandila et al.[56] presented a model of the integrated gasification system using Aspen Plus. Lan et al. [57] developed a model based on Aspen Plus for an integrated system power generation constituted by a biomass gasifier and a gas turbine combustion system.

1.2. Motivation of the work

This work proposes a simulation model of a real micro-cogeneration (mCHP) system, based on biomass gasification in a fixed bed downdraft gasifier, coupled with an ICE. The model, developed in Aspen Plus software, is able to simulate the whole cogeneration system, including biomass gasification, syngas cleaning, ICE and thermal recovery. The gasification model is based on the restricted equilibrium model, the ICE is simulated with a turbine, a combustion chamber and a compressor, and the heat exchangers of the heat recovery system are simulated

by using the real geometrical data by means of Aspen Plus "EDR" (Exchanger Design & Rating) tool.
The models available in the literature do not provide accurate predictions of all the outputs of a whole CHP plant, while the present work aims at providing a more comprehensive analysis.
The model is calibrated on the basis of the detailed design parameters of a real mCHP plant, i.e. CMD-ECO20x, consisting of a biomass gasifier coupled with an ICE, characterized by 20.0 kW_{el} of nominal power output.
The system layout description is reported in the System layout section, while the Simulation model section reports the description of the numerical code developed in Aspen Plus environment.
The simulation model has been validated against the experimental data obtained during an extensive experimental campaign, carried out on the real commercial mCHP module, to assess the reliability and robustness of the code. In the Postprocessing of the experimental data section, the equations used for the calculation of the output operating parameters and the assessment of the global performance are reported.
Some parametric analyses are carried out to investigate the effects of the most important parameters on the gasification system.
Both the model validation and the results of the parametric analyses are discussed in detail in the Results and Discussion section.
Summing up, the main motivations of the present work are: i) enriching the literature with further validation of the Restricted Chemical Equilibrium method by experimental data; ii) validation of the novel numerical model, properly developed for a real mCHP plant, by comparison with the experimental data acquired on the whole system, and not on some subsystems; iii) development of a metrological analysis on the experimental data acquired on site.

2. Methods

In this section, the system layout used for the experimental campaign and the numerical simulation model using Aspen Plus software are described. The proposed model is based on the equilibrium correlations and Gibbs free energy minimizations. The extensive experimental campaign allowed to acquire a large number of data, that have been employed to perform a detailed validation of the model.

2.1. System layout

The 3D view and the system layout of the real mCHP CMD-ECO20x are sketched in Figure 2 and Figure 2, respectively. The main mass flows are reported: the parameters in black colour are directly measured during the experimental campaigns, while the red ones are obtained as indirect measurements.
The CMD-ECO20x is a mCHP system powered with biomass, developed by the Italian company Costruzioni Motori Diesel (CMD) S.p.A.. The unit integrates an Imbert downdraft gasifier, syngas cleaning devices, a spark ignition reciprocating ICE and an electrical generator. The Waste Heat Recovery (WHR) is composed by the heat exchangers installed in both the engine cooling circuit and the exhaust gas line. The CMD-ECO20x is designed to process woody material (in form of chips or briquettes) of residual materials from: wood industry (wood dust, wood furniture factory waste, etc.); agro-industry such as the olive oil industry (exhausted olive pomace mixed with sawdust, olive kernel); rice industry (rice husk), canning industry

(chestnut shells and hazelnut shells); pruning of public green areas. The processed biomass is characterized by G30 size (1.50–3.00 cm) with a maximum humidity of 20%.

The mCHPs is able to produce electrical and thermal power up to 20 kW_{el} and 40 kW_{th}, respectively. The system is fully automated, electronically managed in every operation stage from the automatic loading of biomass/residual material tank into to the parallel connection with the national electrical grid.

The processed biomass (wood chips, represented as a green line in Figure 2), is moved from the tank into the chamber of the reactor through the conveyor belt and a loading apparatus, coupled with an auger placed on the top of the gasifier. The gasification reactions convert the raw materials into syngas.

The whole syngas cleaning apparatus (which removes all the ash, char, tar, and water) consists of a cyclone, a cooler and a filter; the cold side of the syngas cooler is water (dark blue line in Figure 2), which is cooled down by a specific radiator (Radiator 1 – for the sake of simplicity, the inlet and outlet air flows have been omitted). The syngas (light blue line in Figure 2) exiting the cleaning section is mixed with fresh air and aspirated by the ICE.

The ICE, through the alternator, produces the electrical energy that can be delivered to the national electric grid, while engine's exhaust gas passes in the thermal recovery section.

The jacket cooling water (red line in Figure 2), which represents the primary circuit of the thermal recovery, is cooled down in two steps. In the first one, it is cooled through a Plate Heat Exchanger (PHE), whose cold side is the water of the secondary circuit of thermal recovery (orange line in Figure 2); in the second step, it is cooled through a specific radiator (ICE Radiator - for the sake of simplicity, the inlet and outlet air flows have been omitted).

Then, the thermal recovery in the PHE represents the low-temperature thermal recovery of the ICE.

The high-temperature thermal recovery is obtained in a Shell&Tube Heat Exchanger (STHE), whose hot side is the exhaust gas exiting the ICE and whose cold side is the water of the secondary circuit. The latter is sent to the thermal storage system installed outside the module and then it is re-pumped to the CMD-ECO20. In order to simulate a thermal load during the experimental campaigns, a specific radiator was used. (Radiator 2 - for the sake of simplicity, the inlet and outlet air flows have been omitted).

For the sake of completeness, Table 1 describes all the parameters reported in Figure 2, including their units and specifying if the measurement procedure is direct or indirect.

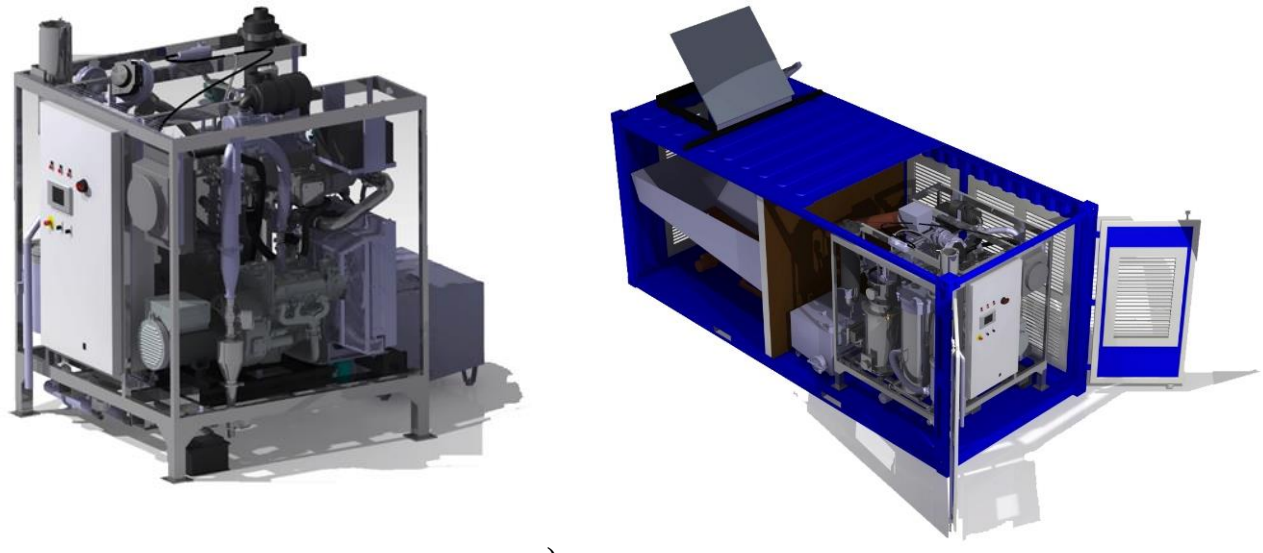

a) b)

Figure 1 3D rendering of the ECO20x; a) reactor, cleaning section, ICE and WHR subsystems; b) the whole ECO20x mCHP unit.

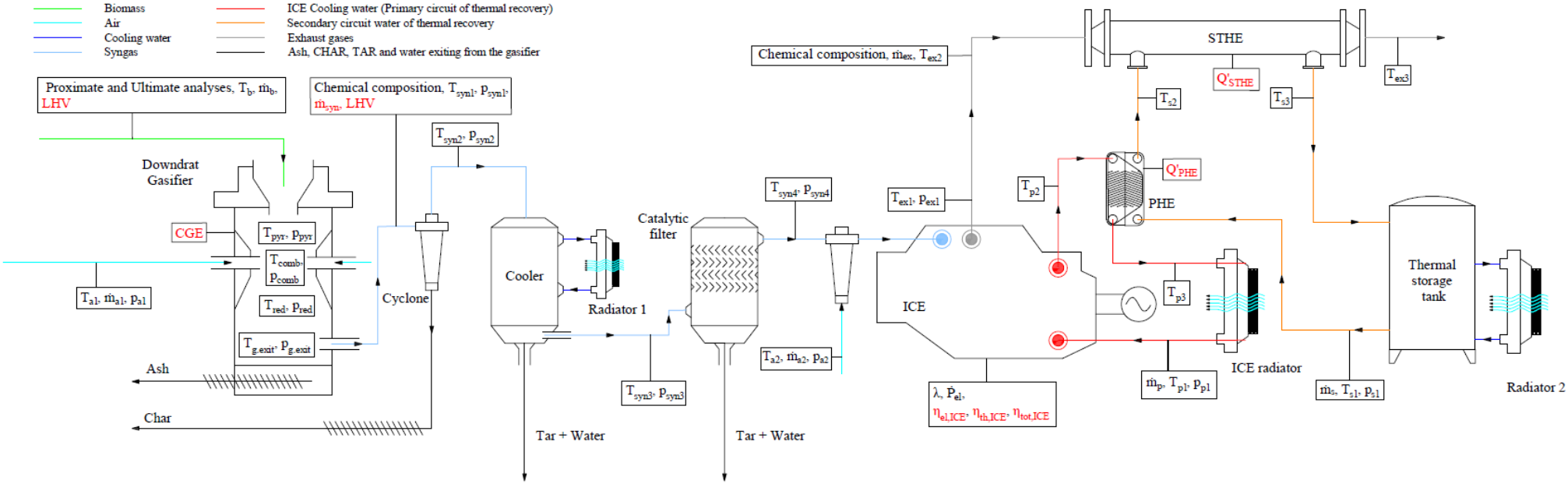

Figure 2 CMD-ECO20 system layout.

468 Table 1 Operating parameters of the CMD-ECO20 system.

Parameter	Description	Unit	Measurement
Biomass			
T_b	Temperature of biomass entering the system	°C	Direct
$\dot{m}_b$	Mass flow rate of biomass entering the system	kg/s	Indirect
LHV_b	LHV of biomass	MJ/kg	Indirect
Air entering the reactor			
T_{a1}	Temperature of the air entering the reactor	°C	Direct
$\dot{m}_{a1}$	Mass flow rate of the air entering the reactor	kg/s	Direct
p_{a1}	Absolute pressure of air entering the reactor	bar(a)	Direct
Inside the gasifier			
T_{pyr}	Temperature inside the reactor in the pyrolysis section	°C	Direct
p_{pyr}	Pressure inside the reactor in the pyrolysis section	bar(g)	Direct
T_{comb}	Temperature inside the reactor in the combustion section	°C	Direct
p_{comb}	Pressure inside the reactor in the combustion section	bar(g)	Direct
T_{red}	Temperature inside the reactor in the reduction section	°C	Direct
p_{red}	Pressure inside the reactor in the reduction section	bar(g)	Direct
$T_{g,exit}$	Temperature at the bottom of the reactor – (Syngas exit)	°C	Direct
$p_{g,exit}$	Pressure at the bottom of the reactor (Syngas exit)	bar(g)	Direct
Syngas			
T_{syn1}	Temperature of syngas entering the cyclone	°C	Direct
p_{syn1}	Pressure of syngas entering the cyclone	bar(g)	Direct
$\dot{m}_{syn}$	Syngas mass flow rate	kg/s	Indirect
LHV_{syn}	LHV of syngas		Indirect
T_{syn2}	Temperature of syngas entering the cooler	°C	Direct
p_{syn2}	Pressure of syngas entering the cooler	bar(g)	Direct
T_{syn3}	Temperature of syngas entering the filter	°C	Direct
p_{syn3}	Pressure of syngas entering the filter	bar(g)	Direct
T_{syn4}	Temperature of syngas entering the ICE	°C	Direct
p_{syn4}	Pressure of syngas entering the ICE	bar(g)	Direct
ICE			
T_{a2}	Temperature of the air entering the ICE	°C	Direct
$\dot{m}_{a2}$	Mass flow rate of the air entering the ICE	kg/s	Direct
p_{a2}	Absolute pressure of air entering the ICE	bar(a)	Direct
λ	Stoichiometric ratio	-	Direct
$\dot{P}_{el}$	Electric power output	kW	Direct
$\eta_{el,ICE}$	ICE electric efficiency	%	Indirect
$\eta_{th,ICE}$	ICE thermal efficiency	%	Indirect
$\eta_{tot,ICE}$	ICE total efficiency	%	Indirect
Water of primary circuit			
T_{p1}	Temperature of primary circuit water entering the ICE	°C	Direct
p_{p1}	Pressure of primary circuit water entering the ICE	bar(g)	Direct
$\dot{m}_p$	Primary circuit water mass flow rate	kg/s	Direct
T_{p2}	Temperature of primary circuit water entering the PHE	°C	Direct
T_{p3}	Temperature of primary circuit water entering the ICE Radiator	°C	Direct
Water of secondary circuit			
T_{s1}	Temperature of secondary circuit water entering the PHE	°C	Direct
p_{s1}	Pressure of secondary circuit water entering the PHE	bar(g)	Direct
$\dot{m}_s$	Secondary circuit water mass flow rate	kg/s	Direct
T_{s2}	Temperature of secondary circuit water entering the STHE	°C	Direct
T_{s3}	Temperature of secondary circuit water exiting the STHE	°C	Direct
Exhaus gases			
T_{ex1}	Temperature of exhaust gases exiting the ICE	°C	Direct
p_{ex1}	Pressure of exhaust gases exiting the ICE	bar(g)	Direct
$\dot{m}_{ex}$	Exhaust gases mass flow rate	kg/s	Indirect
T_{ex2}	Temperature of exhaust gases entering the STHE	°C	Direct

Parameter	Description	Unit	Measurement
T_{ex3}	Temperature of exhaust gases exiting the STHE	°C	Direct
Heat exchangers			
$\dot{Q}_{PHE}$	Thermal power exchanged at the PHE	kW	Indirect
$\dot{Q}_{STHE}$	Thermal power exchanged at the PHE	kW	Indirect
Global system			
$\eta_{el,ECO20}$	Electric efficiency of the whole system	%	Indirect
$\eta_{th,ECO20}$	Thermal efficiency of the whole system	%	Indirect
$\eta_{tot,ECO20}$	Total efficiency of the whole system	%	Indirect

2.2. Simulation model

A model for the cogeneration system, based on biomass gasification, has been implemented in Aspen Plus. Aspen Plus is a commercial software developed by Aspentech [58] to design and simulate many types of industrial processes, using unit operation blocks, such as heat exchangers, separators, pumps, compressors, and reactors. It reproduces steady-state conditions, based on mass and energy relations and phase equilibrium data. This software can predict flow rates, compositions and properties of the streams. The simulation of a process in Aspen Plus involves three main phases: the setting of the flow chart in which the block units and their connections with the relative flows are indicated; the definition of the chemical components of the simulation and the setting of the main parameters of all flows (temperature, pressure, flow rate and composition); the definition of the operating conditions of each block.
The specification of the stream class is an important parameter. In this work, the MIXCINC stream class has been chosen, because the process includes conventional gas and liquid components, conventional solid components (such as solid carbon) and unconventional solid components (such as biomass and ash). The biomass is considered as an unconventional solid, whose chemical composition is defined by the ultimate and proximate analyses.
HCOALGEN and DCOALIGT algorithms were used for enthalpy and density calculation for biomass and ash, using the data from proximate, ultimate and sulfur analyses.
The Peng-Robinson's equation of state with the Boston-Mathias modifications has been used to estimate all physical properties of the conventional components in the gasification process.
The whole CHP model developed in Aspen Plus has been divided into several units: gasifier, syngas cleaning system, ICE and heat recovery system. The flow chart of the system studied in the present paper is reported in the Appendix (Figure A.1).
Table 2 shows the description of the Aspen operation units used for the whole system.

Table 2 Description of the Aspen Plus operation units.

Aspen Plus Name	Block name	Description
RYIELD	DECOMP	Models a reactor by specifying reaction yields of each component, but the reaction stoichiometry and kinetics are unknown.
RGIBBS	GASIFIER	Models a reactor in which equilibrium conditions are reached by minimizing the Gibbs free energy.
SSPLIT	CYCLON	Used to separate solid and gas.
HEATER	COOLER HX	Used for heat exchangers in which is known the temperature of the process.
FLASH 2	SEPARAT	Used to perform calculations related to the liquid-vapor balance.
MIXER	MIX	Used to combine multiple flows of matter or energy.
COMPRESSOR	COMPRESS	Simulates a Compressor
TURBINE	COMBUST	Simulates a Turbine

HEATX	COOL	Simulates Heat Exchanger
	STHE	Simulates Heat Exchanger
	PHE	Simulates Heat Exchanger

2.2.1. Gasifier

The gasification model has been developed in Aspen Plus using a combination of two blocks: the biomass decomposition and the gasification of biomass with air as an oxidant agent. An equilibrium zero-dimensional model is considered where the reactor is perfectly mixed and it is based on the Gibbs free energy minimization. The model is non-stoichiometric, considering that reaction rates and residence times are long enough to reach equilibrium.

The biomass gasification model takes into account the following assumptions:

- steady-state and isothermal model;
- zero-dimensional and kinetic- free model;
- all the gases involved in the reactions are considered ideal gases;
- the char contains only carbon;
- S and N reactions are not considered;
- tar formation has been neglected;
- instantaneous devolatilization of the biomass is considered;
- volatile products considered are H_2, CO, CO_2, CH_4 and water (H_2O);
- the chemical reactions in the gasifier are in an equilibrium state;
- the heat loss has been neglected.

Figure 3 shows the Aspen Plus flowsheet of the biomass gasification system.

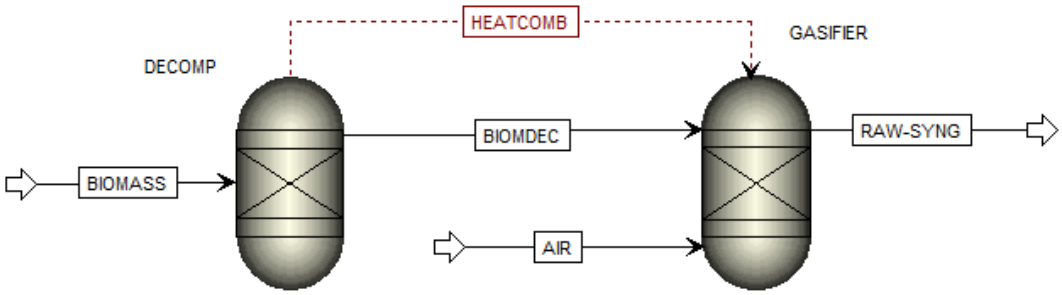

Figure 3 Flowsheet of Aspen Plus® biomass gasification system.

The gasification model consists of two phases: decomposition and gasification. In the biomass decomposition phase, a RYIELD reactor (DECOMP) has been used to decompose the biomass stream (BIOMASS) into its constituent elements, including carbon (C), hydrogen (H_2), oxygen (O_2), nitrogen (N_2), sulfur (S) and ash, by specifying the yield distribution according to the ultimate analysis of biomass, written by Fortran subroutine in a calculator block. The yield distribution is a necessary procedure due to the inability of the RGibbs reactor to deal with non-conventional components such as biomass.

The reaction heat associated with the decomposition of the biomass has been supplied in the RGibbs reactor through a heat flow (QCOMB).

The gasification phase is performed in a RGibbs reactor (GASIFIER) that uses the Gibbs free energy minimization as a model for the chemical equilibrium. This reactor calculates the

composition of the produced gas by minimizing the Gibbs free energy and reaching a complete chemical equilibrium. In this block, the air is introduced as a gasification agent, through the AIR stream.

The reactions considered in the RGibbs reactor (R1-R4) are reported in Table 3. Table 4 reports the main parameters of the gasifier, while Table 5 reports the results of the ultimate and proximate analyses of the biomass used for the experimental campaign, and it is employed as input data in the numerical model.

In the present work, the Restricted Chemical Equilibrium is employed to specify the chemical reactions with different Temperatures approach (specifying a determined Temperature approach for each reaction). The RGibbs reactor evaluates the chemical equilibrium constant at $T + \Delta T approach$, where T is the real reactor temperature (specified in the settings) and $\Delta T approach$ is the Approach Temperature, which represents the difference between the chemical equilibrium Temperature and the real reactor temperature. This method is used to modify the chemical equilibrium, to properly simulate the non-equilibrium conditions of a real gasifier, such as carried out by Gumz [59] and de Andrés [60].

Table 3 Gasification reactions.

Reaction	Description	
$C + 2H_2 \rightarrow CH_4$	Methanation	R1
$CO+H_2O \rightarrow CO_2+ H_2$	CO shift	R2
$H_2 + 0.5\ O_2 \rightarrow H_2O$	Hydrogen Combustion	R3
$C + H_2O \rightarrow CO + H_2$	Water gas shift	R4

Table 4 Gasifier input parameters.

Parameter	Value
Reactor Temperature	800 °C
Pressure	1.02 bar(a)
Air flow rate ($\dot{m}_{a1}$)	8.07×10^{-3} kg/s
Biomass flow rate ($\dot{m}_b$)	6.05×10^{-3} kg/s

Table 5 Biomass proximate and ultimate analyses.

Wood chips					
Proximate Analysis, %		**Ultimate Analysis, %**			
			dry basis	ash and moisture free	as received
Moisture	9.80	Carbon	43.6	43.7	39.4
Fixed Carbon	18.3	Hydrogen	5.20	5.20	4.70
Volatile Matter	71.7	Nitrogen	0.200	0.200	0.200
Ash	0.200	Ash	0.200		0.200
		Oxygen	50.8	50.9	45.8
		Moisture	-	-	9.80

2.2.2. Syngas Cooling and Cleaning System

The syngas cooling and cleaning system has been developed in Aspen Plus using three blocks: a separator SSPLIT type, a separator FLASH2 type and a heat exchanger HEATER type as shown in Figure 4.

The raw syngas (RAW-SYNG) is sent in a SSPLIT separator (CYCLON) in which solid parts are separated from the gas. Indeed, the unreacted char and the ashes (ASH) fall to the bottom, while the syngas comes out from above (SYNGAS). The separated syngas achieves a HEATER block (COOLER) which simulates a water scrubber cooler of the real system, used to cool the syngas, because the internal combustion engine needs gas at a lower temperature compared to the one exiting the gasifier.
The cooled syngas is sent to a further separator Flash2 (SEPARAT) that ensures the separation of the liquid and vapor phase. It is used to separate the syngas from tar (TAR), which is considered composed only of water. Table 6 reports the operating conditions of the syngas cooling and cleaning system.

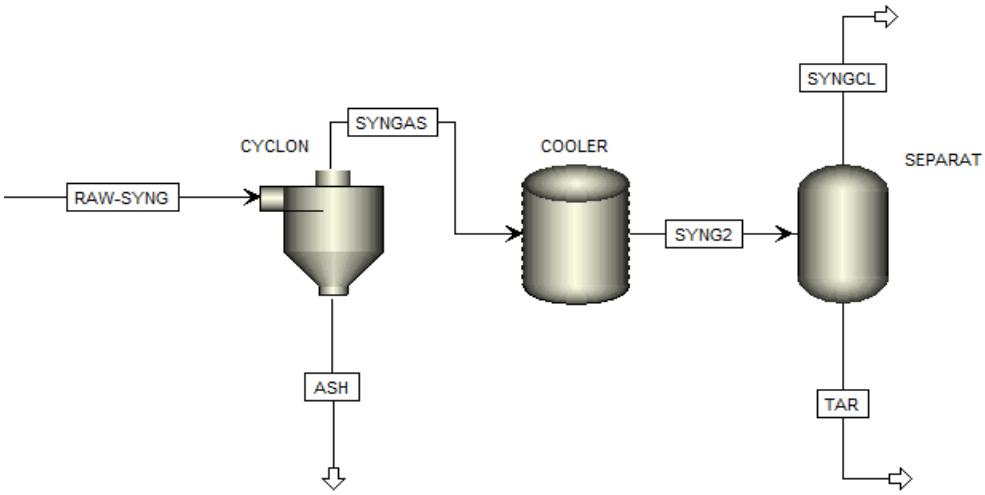

Figure 4 Flowsheet of Aspen Plus® syngas cleaning system.

Table 6 Input parameters of the syngas cooling and cleaning system.

Block unit	Parameter	Value
COOLER	Temperature (T_{syn3})	53.3°C
	Pressure	1.02 bar(g)
SEPARAT	Temperature (T_{syn4})	47.6°C
	Pressure	1.02 bar(g)

2.2.3. Internal Combustion Engine

After the cleaning system, the syngas cleaned (SYNGCL) is mixed with air (AIRICE) in the MIXER block (MIX), then the mixture of air and syngas is aspirated by the ICE. In Aspen Plus database unit block for ICE is not available. Therefore, to simulate the ICE, three blocks that are present in Aspen library have been considered: a compressor, a reactor RGIBBS and a turbine, as shown in Figure 5, representing the engine cycle.
The COMPRESSOR block is used to simulate the compression phase, the reactor RGIBBS is used to simulate the combustion phase and the TURBINE block is used to simulate the expansion phase.
The mixture of air and syngas is sent to the compressor (COMPRESS), ensuring an isentropic process and defining a compression ratio of 9.45, equivalent to the compression ratio of the real

engine. The gas after the compressor is sent to the RGibbs reactor (COMBUST) that simulates the combustion chamber and where combustion reactions occur considering the equilibrium reactions and Gibbs free energy minimization. The exhaust gases generated are sent to the turbine (TURBINE) used to simulate the expansion process, where the power generation stage takes place. For the Turbine block, it is always necessary to define an isentropic expansion and to consider a discharge pressure equal to the atmospheric pressure.
Table 7 reports the input parameters of the ICE employed in the model.

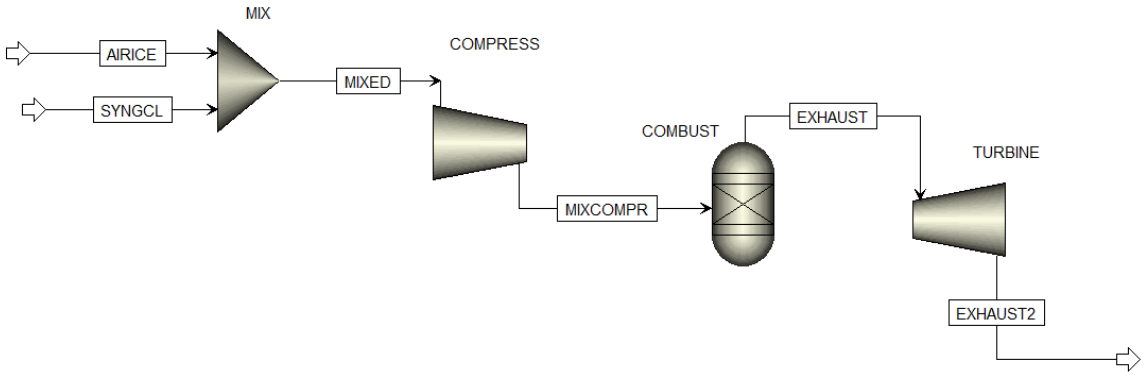

Figure 5 Flowsheet of Aspen Plus® Internal Combustion Engine.

Table 7 Input parameters of the Internal Combustion Engine.

Block unit	Parameter	Value
COMPRESSOR	Isentropic Efficiency	0.85
	Mechanical Efficiency	0.99
	Compression ratio	9.45
TURBINE	Isentropic Efficiency	0.87
	Mechanical Efficiency	0.99
	Pressure discharge	1.00 bar
RGIBBS	Temperature	1430 °C
	Pressure	20.0 bar

2.2.4. Heat Recovery System

The heat recovery system of the CHP plant consists of two heat exchangers: a PHE and a STHE. The thermal energy is recovered from the enthalpy of the exhaust gases using the STHE and from the engine cooling system using the PHE. The PHE is in counter-current configuration, in which the "primary circuit" is referred to water flow of the engine cooling circuit (MICEIN); while in the STHE, in counter-current configuration, flow the exhaust gases of the engine and the user water. The circuit of the user water (MSEC) is named "secondary circuit".
The plate and shell and tube heat exchangers of the heat recovery system have been modeled by using an additional Aspen Plus "EDR" tool, assuming the real geometries taken from the manufacturer datasheets. The flowsheet of the heat recovery system modeled in Aspen Plus is shown in Figure 6. The heat exchangers of the thermal recovery system created with EDR have been modeled in Aspen Plus with two HEATX blocks for the Shell and Tube Heat Exchanger and

Plate Heat Exchanger. A third exchanger HEATX block (COOL) has been used to simulate the cooling system of the engine using the water of the engine cooling jacket (MICEIN).
The user water (MSEC1) is first heated by the water of the engine cooling circuit (MICEOUT1) in the plate exchanger, then, after exiting from the plate exchanger (MSEC2), recovers other thermal energy through the exhaust gases coming out from the engine (EXHAOUT) in the STHE. In the pilot system, during the experimental campaign, the user water is cooled by a radiator (RADIAT1), able to dissipate the heat necessary to return to the initial temperature T_{s1}, while the water of the primary circuit exiting the PHE (MICEOUT2) was cooled in the engine radiator (RADIAT2), reaching engine inlet Temperature T_{p1}.
In Table 8, the Heat Recovery System input parameters are reported. For the sake of clarity, all the input data of the numerical model and all the outputs of every single subsystem are reported in Table 9 and Table 10, respectively.

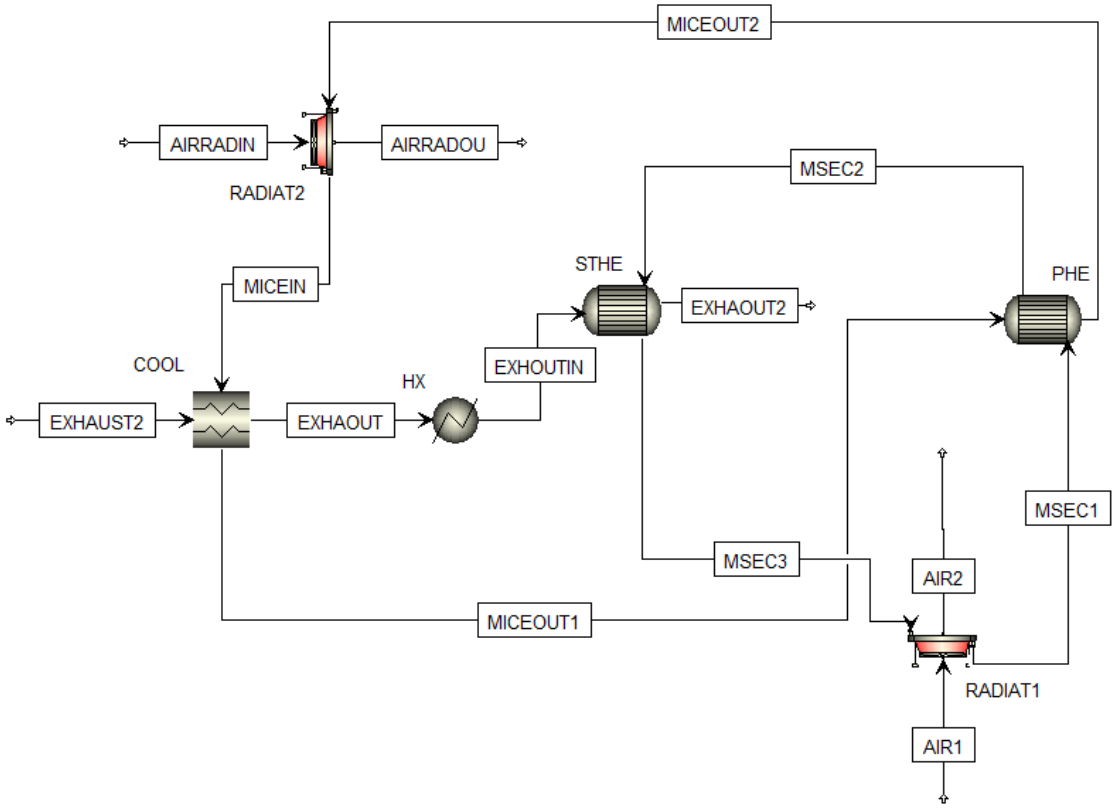

Figure 6 Flowsheet of Aspen Plus® Heat Recovery System.

Table 8 Input parameters of the Heat Recovery System.

Block unit	Parameter	Value
COOL	Engine cooling water flow rate ($\dot{m}_p$)	0.137 kg/s
	Temperature of water at inlet the engine (T_{p1})	49.1 °C
PHE	User water flow rate ($\dot{m}_s$)	0.344 kg/s
	Temperature of user water at inlet PHE (T_{s1})	58.6 °C

Table 9 Input data of the simulation model.

Parameter	Description
Biomass	
$\dot{m}_b$ (kg/s)	Mass flow rate of biomass entering the system
T_b (°C)	Temperature of biomass entering the system
p_b (bar(a))	Absolute pressure of biomass entering the reactor
Proximate Analysis of biomass (%)	
Ultimate Analysis of biomass (%)	
Air entering the reactor	
$\dot{m}_{a1}$ (kg/s)	Mass flow rate of the air entering the reactor
T_{a1} (°C)	Temperature of the air entering the reactor
p_{a1} (bar(a))	Absolute pressure of air entering the reactor
Gasifier	
T_{red} (°C)	Temperature inside the reactor in the reduction section
p_{red} (bar(g))	Pressure inside the reactor in the reduction section
Syngas Cooling System	
T_{syn3} (°C)	Temperature of syngas entering the filter
p_{syn3} (bar(g))	Pressure of syngas entering the filter
T_{syn4} (°C)	Temperature of syngas entering the ICE
Water of primary circuit	
T_{p1} (°C)	Temperature of primary circuit water entering the ICE
p_{p1} (bar(g))	Pressure of primary circuit water entering the ICE
$\dot{m}_p$ (kg/s)	Primary circuit water mass flow rate
Water of secondary circuit	
T_{s1} (°C)	Temperature of secondary circuit water entering the PHE
p_{s1} (bar(g))	Pressure of secondary circuit water entering the PHE
$\dot{m}_s$ (kg/s)	Secondary circuit water mass flow rate

Table 10 Output data of the simulation model

Parameter	Description
Syngas	
$\dot{m}_{syngas}$ (kg/s)	Syngas mass flow rate
LHV_{syn} (MJ/kg)	LHV of syngas
Syngas Composition mol (%)	Syngas Composition
ICE	
T_{a2} (°C)	Temperature of the air entering the ICE
p_{a2} (bar(a))	Absolute pressure of the air entering the ICE
$\dot{P}_{el}$ (kW)	Electric power output
λ	Stoichiometric ratio
Primary and secondary circuit	
T_{p2} (°C)	Temperature of primary circuit water entering the PHE
T_{p3} (°C)	Temperature of primary circuit water entering the ICE Radiator
T_{s2} (°C)	Temperature of secondary circuit water entering the STHE
T_{s3} (°C)	Temperature of secondary circuit water exiting the STHE

Parameter	Description
Exhaust gases	
T_{ex1} (°C)	Temperature of exhaust gases exiting the ICE
T_{ex2} (°C)	Temperature of exhaust gases entering the STHE
$\dot{m}_{ex}$	Exhaust gases mass flow rate
T_{ex3} (°C)	Temperature of exhaust gases exiting the STHE
p_{ex1} (bar(g))	Pressure of exhaust gases exiting the ICE
Heat exchangers	
$\dot{Q}_{PHE}$ (kW)	Thermal power exchanged at the PHE
$\dot{Q}_{STHE}$ (kW)	Thermal power exchanged at the PHE

2.3. Settings of the experimental campaign

The results obtained from the simulation model have been validated against the real experimental data collected during an experimental campaign aimed at characterizing the performance of the ECO20 system.
In particular, three different operating parameters have been varied during the tests, as reported in Table 11:
- the stoichiometric ratio, λ;
- the ignition timing, expressed in degrees before the top dead center (BTDC);
- the power of the pump of the thermal recovery secondary circuit.

The first and second parameters allowed to know the best operating conditions in terms of maximum electric and global efficiency; the third parameter has been varied to characterize the heat exchanger operations, focusing in particular on the cooling of the ICE.

Table 11 Test carried out during the experimental campaign.

	BTDC [°]	λ [-]	Pump power
1	34	1.010	maximum
2	29	1.010	maximum
3	24	1.010	maximum
4	24	1.110	maximum
5	29	1.110	maximum
6	34	1.110	maximum
7	34	1.050	maximum
8	29	1.050	maximum
9	24	1.050	maximum
10	29	1.010	medium
11	29	1.010	minimum

2.4. Postprocessing of the experimental data

Once all the data coming from the experimental campaigns have been collected, the postprocessing has been carried out, in order to assess the operating values of the parameters obtained using indirect measurements.
For the sake of brevity, only the main equations used for postprocessing are reported below.

$$\dot{m}_b = \frac{m_b}{\Delta t} \quad \text{kg/s} \quad (1)$$

where m_b is the total biomass rate, expressed in kg/s, processed during the experimental campaign carried out during the period of time Δt (expressed in s); such a relation can be considered only valid under the simplifying assumption of constant feeding of the mCHP module.

Firstly, the overall primary power related to the biomass $\dot{E}_b$ entering the system is obtained.

$$\dot{E}_b = (\dot{m}_b \, LHV_b) \cdot 1000 \quad \text{kW} \quad (2)$$

Where LHV_b is the Lower Heating Value of the biomass ("as received") expressed in MJ/kg and obtained as follow [61], [62]:

$$LHV_b = HHV_{ar} \; 2.433 \cdot \left(8.936 \cdot \frac{H}{100} \cdot \left(1 - \frac{W}{100} \right) + \frac{W}{100} \right) \quad \text{MJ/kg} \quad (3)$$

$$HHV_{ar} = HHV_{dry} \cdot \left(1 - \frac{W}{100} \right) \quad \text{MJ/kg} \quad (4)$$

$$HHV_{dry} = 0.349 \cdot C + 1.1783 \cdot H + 0.1005 \cdot S - 0.1034 \cdot O - 0.0151 \cdot N - 0.0211 \cdot A \quad \text{MJ/kg} \quad (5)$$

where the letters C, H, S, O, N, and A represent the mass percentages on a dry basis of carbon, hydrogen, sulfur, oxygen, nitrogen and ash of the biomass, respectively; W is the water content.
The ER is a relevant gasification parameter affecting the syngas quality and it is defined as:

$$ER = \frac{\text{Actual Air}}{\text{Stoichiometric Air}} = \frac{(\text{Air}/\text{Fuel})}{(\text{Air}/\text{Fuel})\text{stoich}} \quad (6)$$

The primary power related to the syngas $\dot{E}_{syn}$ entering the ICE is obtained as:

$$\dot{E}_{syn} = (\dot{m}_{syn} \, LHV_{syn}) \cdot 1000 \quad \text{kW} \quad (7)$$

Once the chemical composition of the syngas is known, as well as its specific stoichiometric AirFuel ratio α_{st}, it is possible to calculate both the LHV_{syn} and the mass flow rate $\dot{m}_{syn}$.
The LHV is obtained as:

$$LHV_{syn} = \sum_i y_i \, LHV_i \quad \text{MJ/kg} \quad (8)$$

where y_i represents the mass fraction of the i^{th} syngas component and LHV_i its specific LHV expressed in MJ/kg
The mass flow rate is obtained as:

$$\dot{m}_{syn} = \frac{\dot{m}_{ex}}{1 + \lambda \alpha_{st}} \quad \text{kg/s} \quad (9)$$

where $\dot{m}_{ex}$ is the mass flow rate of the exhaust gases exiting the ICE, λ is the operating stoichiometric ratio (measured by the on board detection system) and α_{ST} is the stoichiometric air-fuel ratio, which is calculated as:

$$\alpha_{st} = \sum_{i=1}^{n} y_i \cdot \alpha_{st,i} \quad \text{kg/s} \quad (10)$$

where y_i is the mass fraction of the i_{th} chemical species present in the syngas and $\alpha_{ST,i}$ is its specific air-fuel ratio.

The gasifier Cold Gas Efficiency (CGE) is obtained as:

$$CGE = \frac{\dot{E}_{syn}}{\dot{E}_b} \quad (11)$$

Thermal power exchanged in the heat exchangers is obtained as follow (considering only the cold side):

$$\dot{Q}_{PHE} = \dot{m}_s \cdot c_p \cdot (T_{s2} - T_{s1}) \quad \text{kW} \quad (12)$$

$$\dot{Q}_{STHE} = \dot{m}_s \cdot c_p \cdot (T_{s3} - T_{s2}) \quad \text{kW} \quad (13)$$

Finally, all the efficiencies of the ICE (Eq. 13, 14, and 15) and ECO20 module (Eq. 16, 17, and 18) can be assessed:

$$\eta_{el,ICE} = \frac{\dot{P}_{el}}{\dot{E}_{syn}} \quad (14)$$

$$\eta_{th,ICE} = \frac{\dot{Q}_{PHE} + \dot{Q}_{STHE}}{\dot{E}_{syn}} \quad (15)$$

$$\eta_{tot,ICE} = \eta_{el,ICE} + \eta_{th,ICE} \quad (16)$$

$$\eta_{el,ECO20} = \frac{\dot{P}_{el}}{\dot{E}_b} \quad (17)$$

$$\eta_{th,ECO20} = \frac{\dot{Q}_{PHE} + \dot{Q}_{STHE}}{\dot{E}_b} \quad (18)$$

$$\eta_{tot,ECO20} = \eta_{el,ICE} + \eta_{th,ICE} \quad (19)$$

2.5. Metrological analysis

A metrological analysis has been carried out on the experimental data. Type A and Type B uncertainties have been associated with the experimental measurements to calculate the combined uncertainty [63], [64]. Then, a coverage factor equal to one has been used to obtain the expanded combined uncertainty, corresponding to a confidence level of 68.3%, based on Gauss distribution.
As regards the calculation of Type A uncertainty, the authors have considered the acquisition of one measure per second, for intervals of 3 minutes, obtaining 180 data per interval.

$$u_A(X_i) = \sqrt{\frac{1}{n(n-1)} \sum_{j=1}^{n} \left(x_j - \bar{x} \right)^2} \tag{20}$$

As concerns the calculation of Type B uncertainty, this has been based on the specifications of the instruments declared by the manufacturer, reported in Table 12.

Table 12 Technical specifications of the probes employed for the thermo-fluid dynamic measurements

Measured quantity	**Instrument**	**Measured range**	**Accuracy**
Air mass flow rate	Hot-film	0 to 1080 kg/h	±4.00% r.v.
Water mass flow rate	Turbine flow meter	0 to 30 l/min	±1.00% r.v
Temperature	K-type thermocouple	-40°C to +1200°C	max(1.50; 0.004×t)
Relative pressure	Piezoresistive transducer	-25.0 to +25.0 kPa	±5.00% r.v
Absolute pressure	Piezoresistive transducer	15.0 to 115 kPa	±1.50% r.v
Relative humidity range	Hygrometer	0 to 100%	±3.00% r.v.

Therefore, the combined uncertainty has been calculated as:

$$u_c\left(X_i\right) = \sqrt{u_A{}^2(X_i) + u_B{}^2(X_i)} \tag{21}$$

The combined uncertainty for indirect measurements has been obtained as:

$$u_c(Y) = \sqrt{\sum_{i=1}^{N} \left(\frac{\partial Y}{\partial X_i} \right)^2 \cdot u^2(X_i)} \tag{22}$$

Finally, the expanded combined uncertainty has been calculated as:

$$U_c(X) = k \cdot u_c(X) \tag{23}$$

where *k* is the coverage factor, which, in this analysis, has been assumed equal to one, corresponding to a confidence level of 68.3%.

2.6. Sensitivity analyses

The sensitivity analyses have been carried out to investigate the influence of relevant parameters on the biomass gasification process. In particular, the effects of gasification temperature, equivalence ratio and moisture content of biomass on the gasification process have been considered.
ER and gasification temperature have been varied to investigate the effects on the syngas molar composition and LHV of the syngas. ER has been varied between 0.1 and 1, with a step of 0.1. The gasification temperature has been varied between 760 °C and 970°C, with a step of 30.0 °C. The biomass moisture content (MC) of biomass has been varied from 5.00% to 40.0%, with a step of 2.50%. Moreover, to investigate the effects of MC on the syngas molar composition and syngas LHV, the effect of MC on the Electrical Power of the engine has been evaluated.

3. Results and Discussion

The numerical model has been validated against the experimental data collected during an extensive experimental campaign. Sensitivity analyses have been performed with the aim of investigating the influence of various parameters on the results.

3.1. Experimental campaign

The main measured parameters deriving from the experimental campaign are reported in Table A.1 and Table A.2 of the Appendix. These parameters have been used to determine the system efficiencies, reported in Table A.3 of the Appendix. The values reported in the Appendix are expressed together with their expanded combined uncertainty, as described in section 2.5.
In particular, the on site tests have allowed to directly measure temperature and mass flow rate values in all the relevant sections of the novel system under investigation, and the results are reported in Table A.1. The description of the measured parameters is reported in Table 1. Moreover, indirect measurements have been performed, and the corresponding results are reported in Table A.2, showing the electric and thermal powers. Based on the values reported in these tables, the system efficiencies have been obtained, as indirect measurements, as reported in Table A.3.

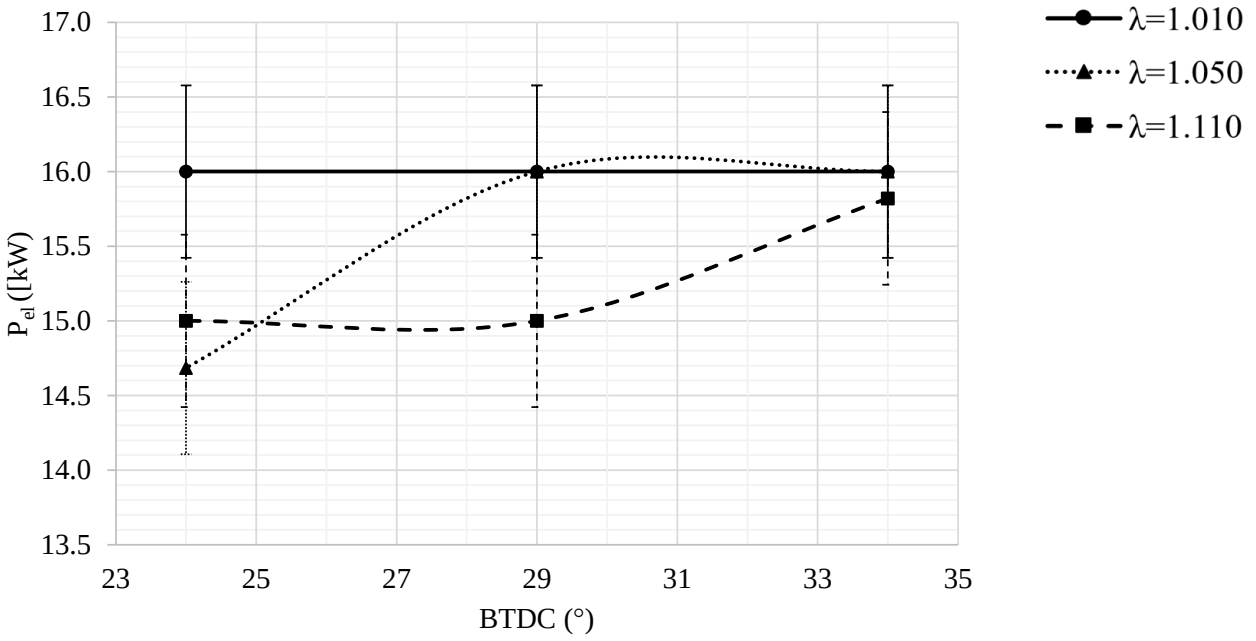
17.0
16.5
16.0
15.5
15.0
14.5
14.0
13.5
P_{el} ([kW)
23
25
27
29
31
33
35
BTDC (°)
λ=1.010
λ=1.050
λ=1.110

a)

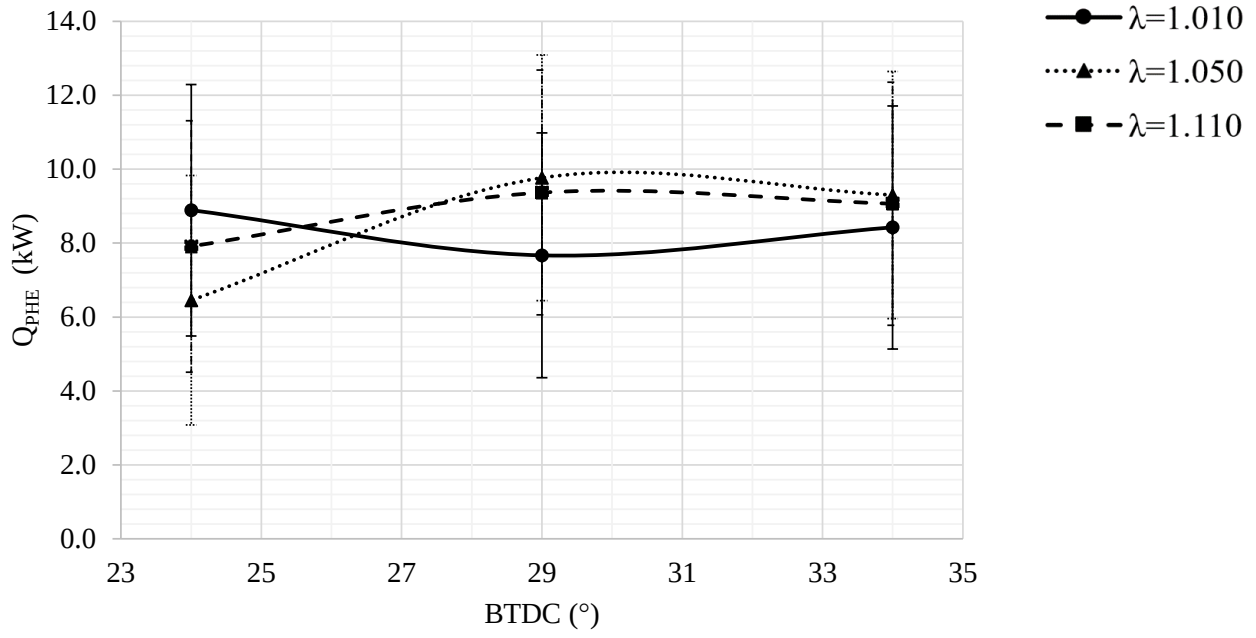
14.0
12.0
10.0
8.0
6.0
4.0
2.0
0.0
Q_{PHE} (kW)
23
25
27
29
31
33
35
BTDC (°)
λ=1.010
λ=1.050
λ=1.110

b)

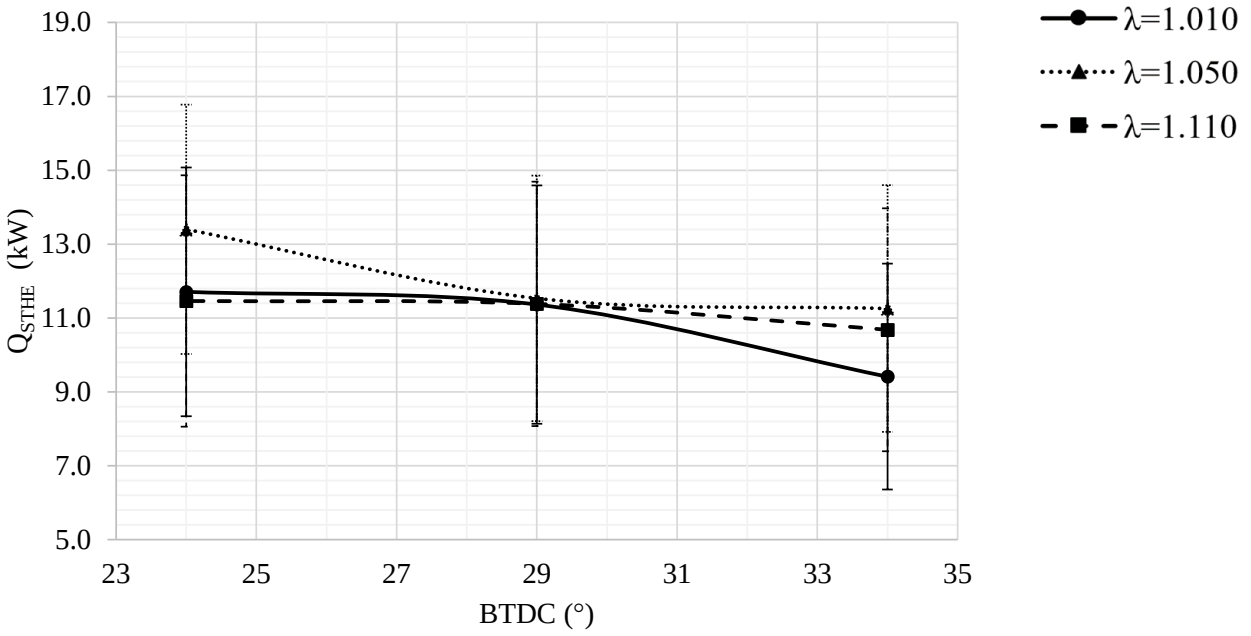
19.0
17.0
15.0
13.0
11.0
9.0
7.0
5.0
Q_{STHE} (kW)
23
25
27
29
31
33
35
BTDC (°)
λ=1.010
λ=1.050
λ=1.110

c)

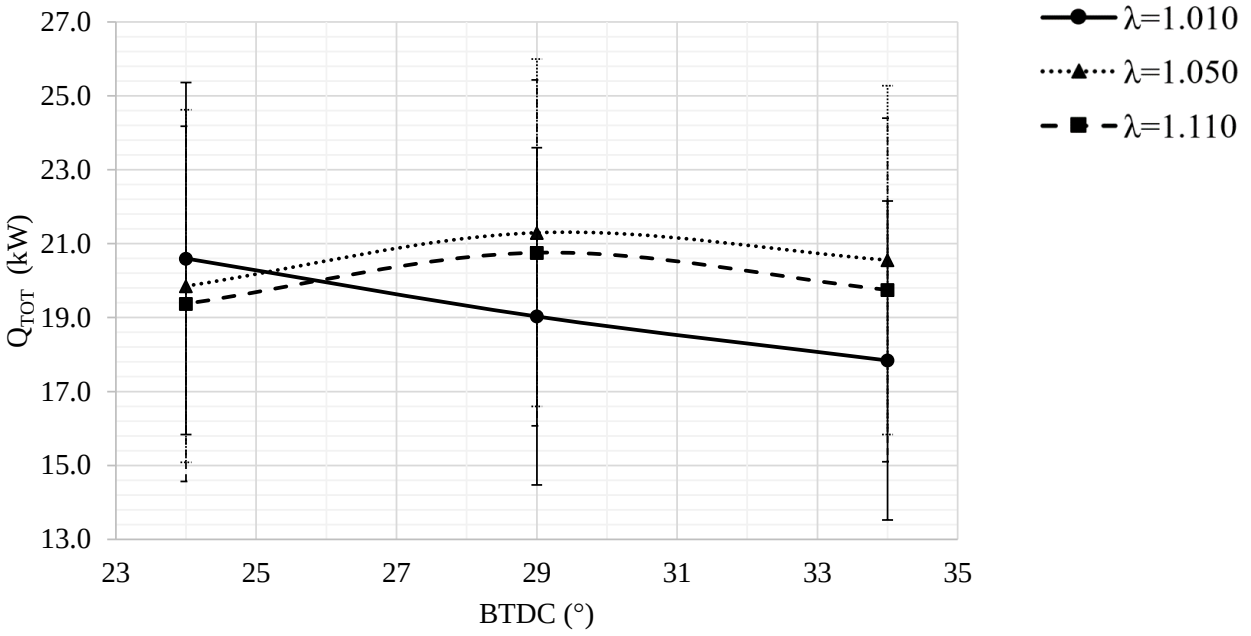
27.0
25.0
23.0
21.0
19.0
17.0
15.0
13.0
Q_{TOT} (kW)
23
25
27
29
31
33
35
BTDC (°)
λ=1.010
λ=1.050
λ=1.110

d)

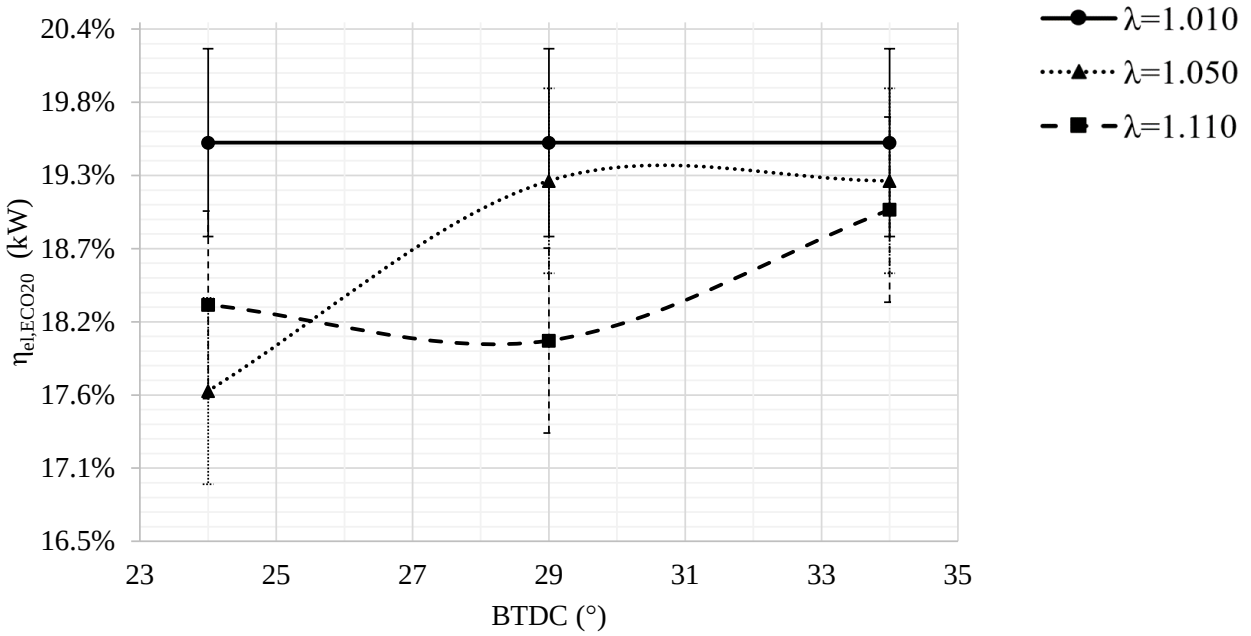
20.4%
19.8%
19.3%
18.7%
18.2%
17.6%
17.1%
16.5%
$\eta_{el,ECO20}$ (kW)
23
25
27
29
31
33
35
BTDC (°)
λ=1.010
λ=1.050
λ=1.110

e)

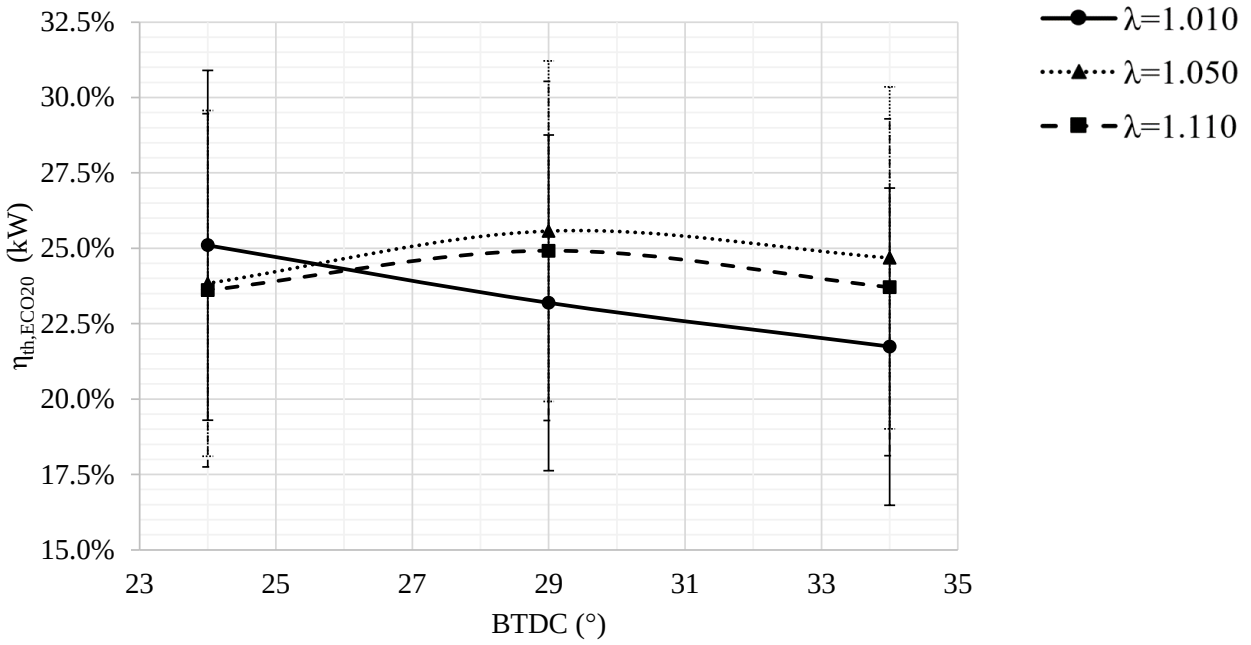
32.5%
30.0%
27.5%
25.0%
22.5%
20.0%
17.5%
15.0%
$\eta_{th,ECO20}$ (kW)
23
25
27
29
31
33
35
BTDC (°)
λ=1.010
λ=1.050
λ=1.110

f)

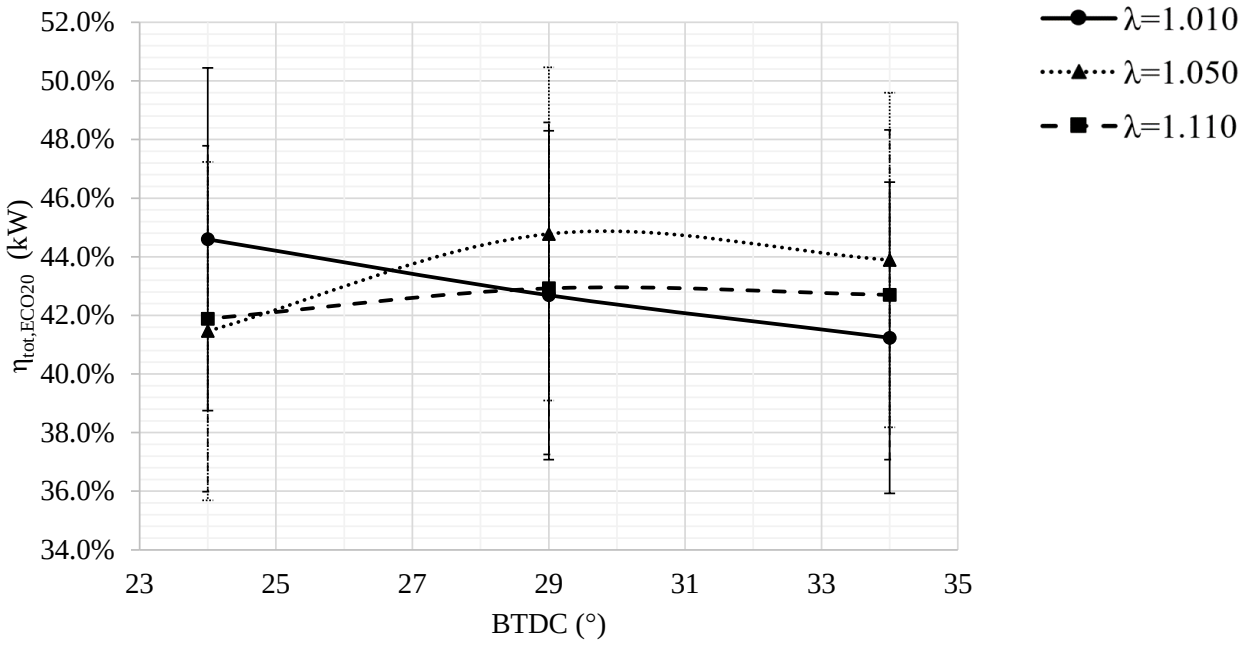

g)

Figure 7 reports the main parameters used to analyze the performance of the system, as function of BTDC and stoichiometric ratio λ.

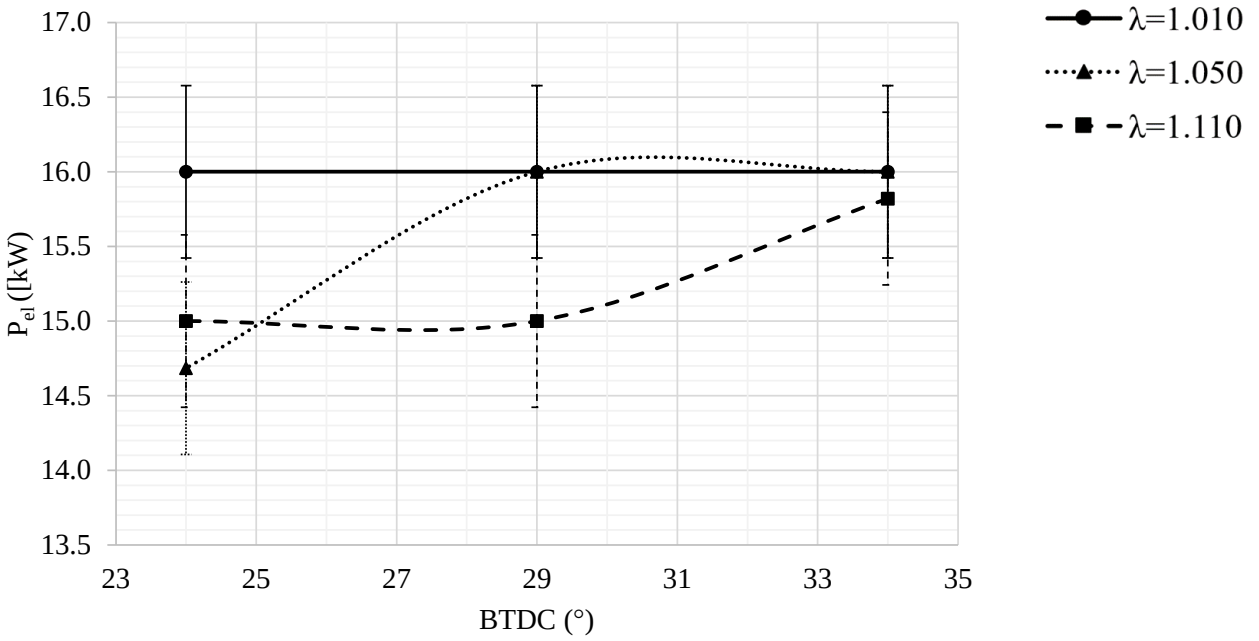

a)

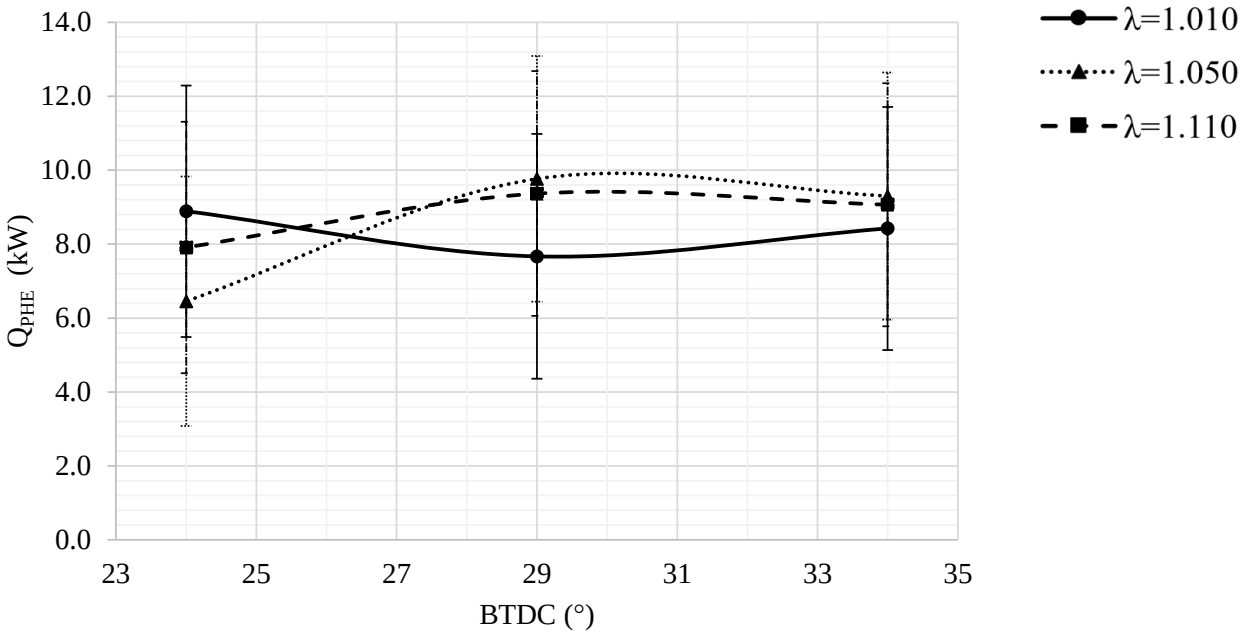
λ=1.010
λ=1.050
λ=1.110
14.0
12.0
10.0
8.0
6.0
4.0
2.0
0.0
Q_{PHE} (kW)
23
25
27
29
31
33
35
BTDC (°)

b)

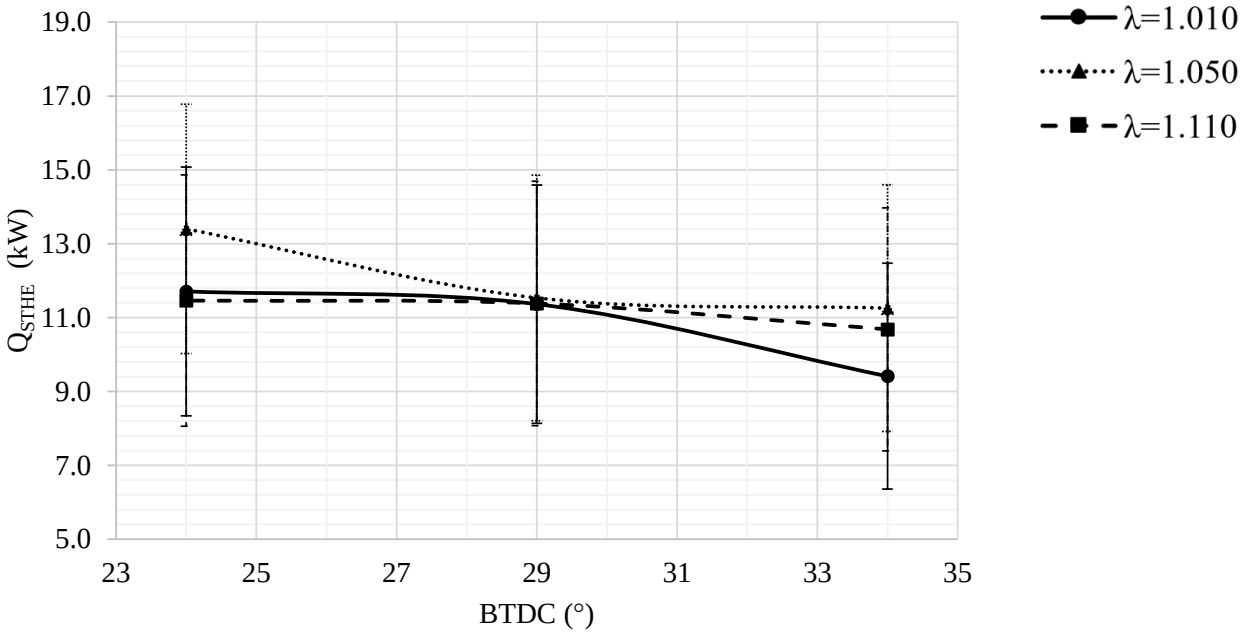
λ=1.010
λ=1.050
λ=1.110
19.0
17.0
15.0
13.0
11.0
9.0
7.0
5.0
Q_{STHE} (kW)
23
25
27
29
31
33
35
BTDC (°)

c)

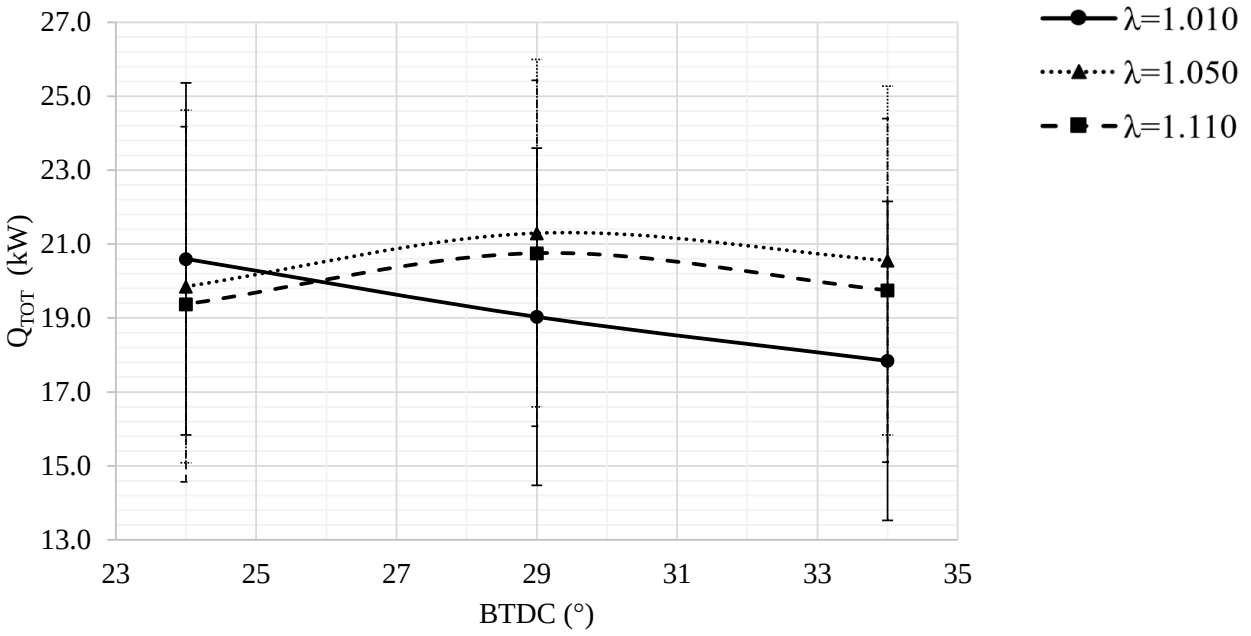
27.0
25.0
23.0
21.0
19.0
17.0
15.0
13.0
Q_{TOT} (kW)
23
25
27
29
31
33
35
BTDC (°)
λ=1.010
λ=1.050
λ=1.110

d)

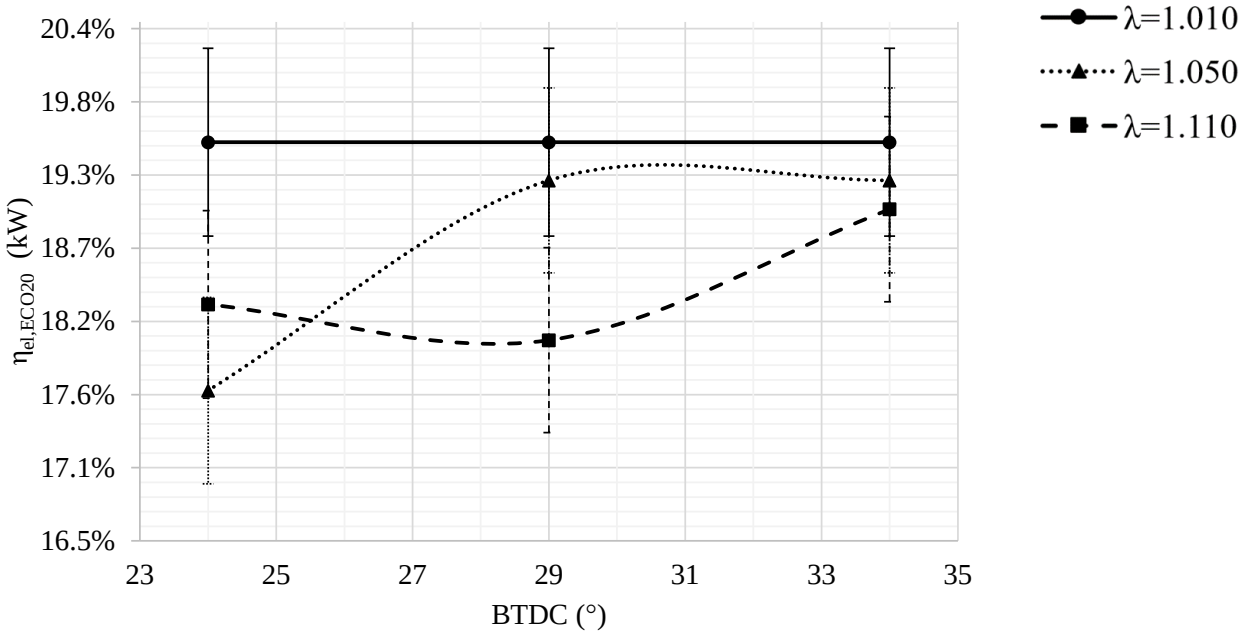
20.4%
19.8%
19.3%
18.7%
18.2%
17.6%
17.1%
16.5%
$\eta_{el,ECO20}$ (kW)
23
25
27
29
31
33
35
BTDC (°)
λ=1.010
λ=1.050
λ=1.110

e)

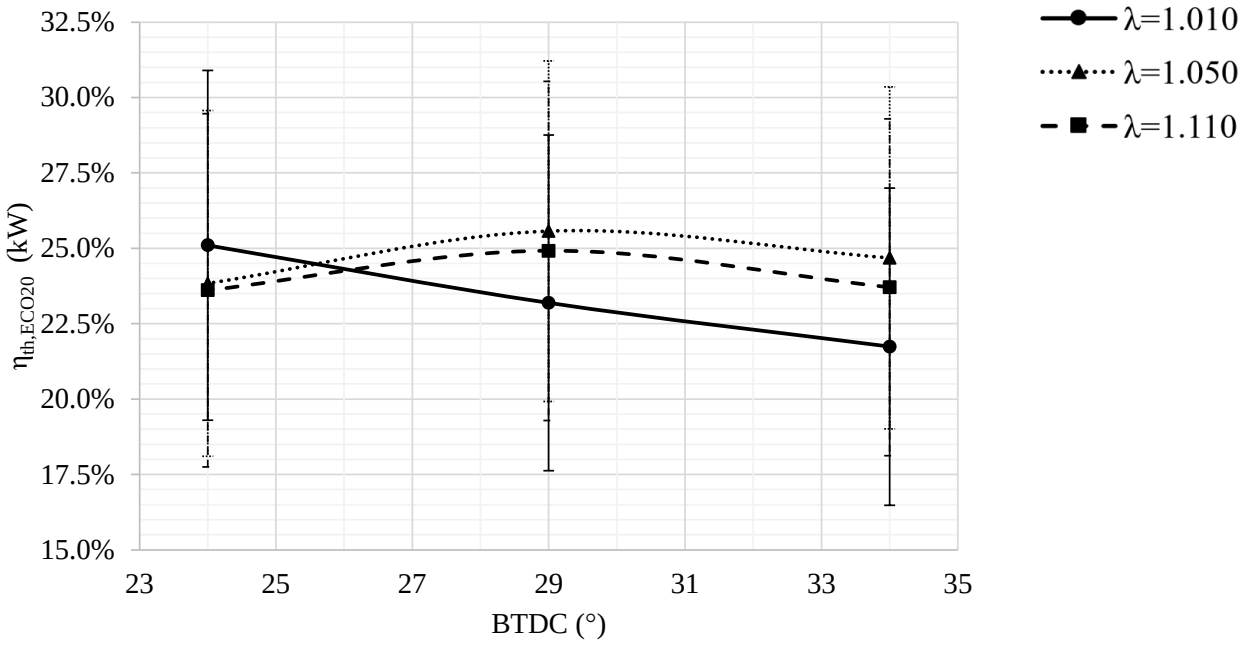

f)

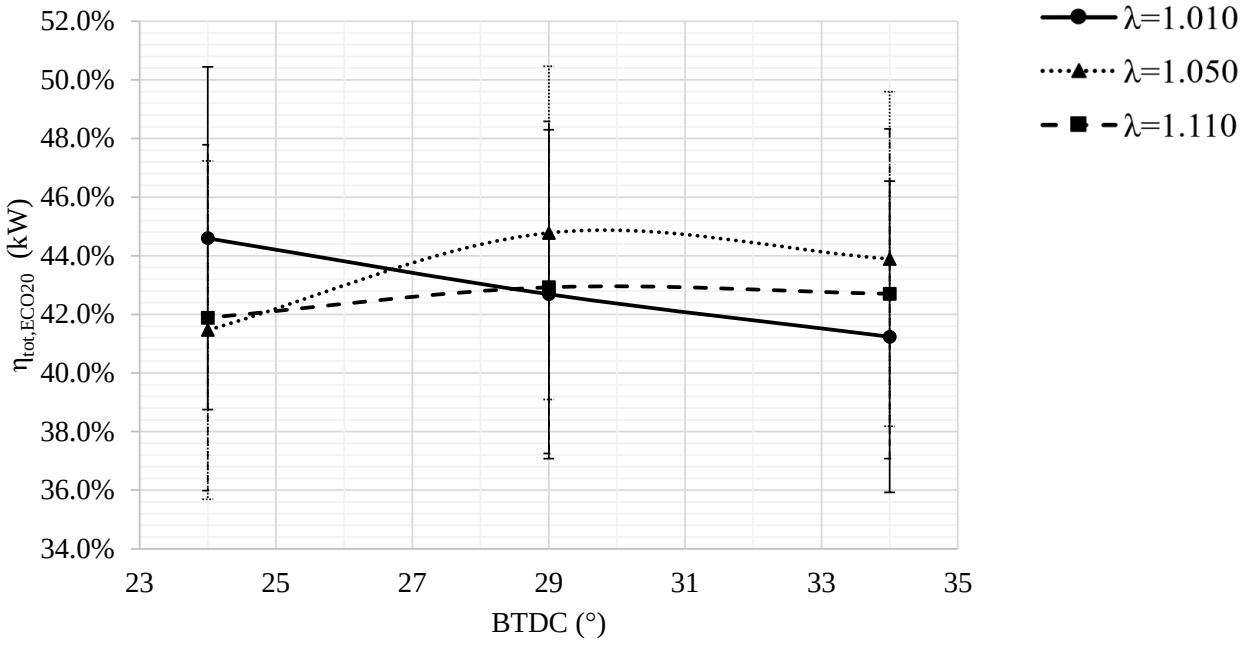

g)

Figure 7 System performance as function of the BTDC and stoichiometric ratio λ: a) electric power produced; b) thermal power recovered at the PHE, c) thermal power recovered at the STHE; d) total thermal power recovered; e) global electric efficiency; f) global thermal efficiency; g) global cogeneration efficiency.

3.2. Model validation

In order to validate the model developed in this work, the numerical results have been compared with the experimental data.

Table 13 and Table 14 report the parameters obtained as direct and indirect measurements, respectively. All the values are reported with the corresponding expanded combined uncertainty, calculated with 68.3% of confidence, i.e. k=1.

Table 13 Main directly measured operating parameters.

Parameter	Value	Parameter	Value
Biomass		*ICE*	
T_b	36.2 ±1.5 °C	λ	1.010 ± 0.007
$\dot{m}_b$	(6.05 ± 0.0080) $\times 10^{-3}$ kg/s	$\dot{P}_{el}$	16.0 ± 0.60 kW
Air entering the reactor		*Syngas*	
T_{a1}	34.2 ±1.5 °C	T_{syn1}	404 ± 1.7 °C
$\dot{m}_{a1}$	(8.07 ± 0.14)$\times 10^{-3}$ kg/s	T_{syn2}	307 ± 1.5 °C
p_{a1}	1.02 ± 0.007 bar	T_{syn3}	53.3 ± 1.5 °C
Inside the gasifier		T_{syn4}	47.6 ± 1.5 °C
T_{pyr}	42.6 ± 1.5 °C	*Exhaust gases*	
T_{comb}	910 ± 4.2 °C	$\dot{m}_{ex}$	
T_{red}	805 ± 3.3 °C	T_{ex1}	338 ± 1.5 °C
$T_{g,exit}$	471 ± 1.9 °C	T_{ex2}	296 ± 1.5 °C
		T_{ex3}	115 ± 1.5 °C
Water of primary circuit		*Water of secondary circuit*	
$\dot{m}_p$	0.137 ±0.0024 kg/s	$\dot{m}_s$	0.344 ±0.0020 kg/s
T_{p1}	49.1 ± 1.5 °C	T_{s1}	58.6 ± 1.5 °C
T_{p2}	74.8 ± 1.5 °C	T_{s2}	64.4 ± 1.5 °C
T_{p3}	57.9 ± 1.5 °C	T_{s3}	71.0 ± 1.5 °C

Table 14 Main indirectly measured operating parameters.

Parameter	Value	Parameter	Value
LHV_b	13.56 ±0.016 MJ/kg	$\dot{Q}_{STHE}$	9.42 ± 3.2 kW
$\dot{E}_b$	82.1 ± 0.22 kW	$\eta_{el,ICE}$	28.1 ± 1.1 %
LHV_{syn}	3.29 ± 0.0000047 MJ/kg	$\eta_{th,ICE}$	31.3 ± 7.6 %
$\dot{m}_{syn}$	(16.2 ± 0.42) $\times 10^{-3}$ kg/s	$\eta_{tot,ICE}$	59.4 ± 7.7 %
$\dot{E}s_{yn}$	57.0 ± 0.55 kW	$\eta_{el,SYST}$	19.5 ± 0.71 %
CGE	65.6 ± 0.70 %	$\eta_{th,SYST}$	21.7 ± 5.3 %
$\dot{Q}_{PHE}$	8.40 ± 3.2 kW	$\eta_{tot,SYST}$	41.2 ± 5.3 %

Table 15 shows the comparison of the numerical results with the experimental data for syngas composition in molar fraction. The calculated and measured values of the syngas characteristics, like LHV and mass flow rate of the syngas, are also reported. The Aspen Plus results obtained in this work, using a Restricted Chemical Equilibrium Model, are in good agreement with experimental results, also considering that the equilibrium model neglects the gasification issues, such as kinetics and fluid dynamics. The comparison between numerical and experimental data has a low percentage deviation for H_2 content (25%), CH_4 content (7%) and N_2 content (23%). The largest difference is found for CO and CO_2 content (percentage deviation is about 40%), for which the Aspen model overestimates the molar fraction of CO and CO_2.

Table 15 Numerical and experimental results in terms of syngas molar composition.

	Experimental	Aspen Model
CO % mol	15.9 ± (5.77 $\times 10^{-6}$)	22.5

	Experimental	Aspen Model
H_2 % mol	12.2 ± (5.77 ×10^{-6})	15.2
CH_4 % mol	1.24 ± (5.77 ×10^{-6})	1.20
CO_2 % mol	9.16 ± (5.77 ×10^{-6})	13.6
N_2 % mol	61.5 ± (5.77 ×10^{-6})	47.5
LHV_{syngas} (MJ/m^3)	3.77 ± (8.46×10^{-6})	4.89
$\dot{m}_{syn}$ (kg/s)	(16.2 ± 0.42)×10^{-3}	13.1×10^{-3}

The heat recovery system has been validated by comparing the temperature values calculated with the model and those obtained through thermocouples on the real plant, as shown in Figure 8. A very good agreement is observed. Moreover, Table 16 reports the calculated and measured values of thermal powers and the main efficiencies of the system. The calculated differences should be considered acceptable, also because the numerical values are within the uncertainty intervals for eight parameters out of nine.

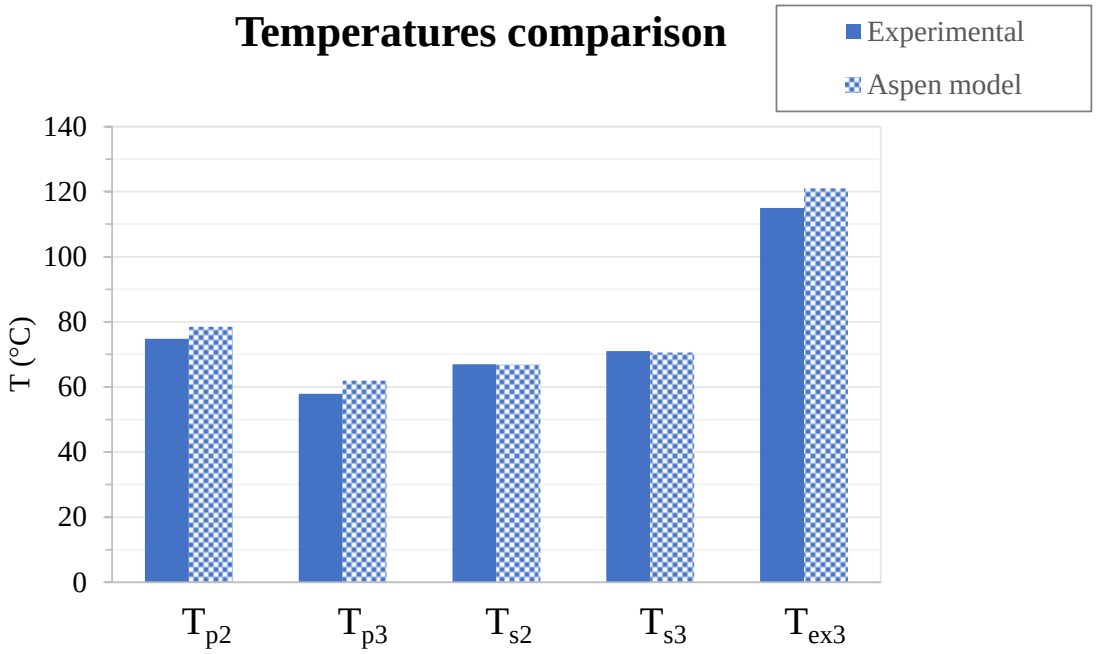

Figure 8 Numerical and experimental results in terms of temperature values in different sections of the system.

Table 16 Numerical and experimental results in terms of temperature values in different sections of the system.

	Experimental	Aspen Model	Difference
Q_{PHE}	8.40 ± 3.2 kW	9.3 kW	11 %
Q_{STHE}	9.42 ± 3.2 kW	5.3 kW	44%
Q_{TOT}	17.8 kW ± 3.2 kW	14.6 kW	18 %
$\dot{P}_{el}$	16.0 ± 0.60 kW	16.3 kW	1.8%
η_{th_ICE}	31.3 ± 7.6 %	26.6 %	15 %
η_{el_ICE}	28.1 ± 1.1 %	29.7 %	5.8 %
η_{TOT_ICE}	59.4 ± 7.7 %	56.3 %	5.0 %
η_{th_SYST}	21.7 ± 5.3 %	17.8 %	18 %

	Experimental	Aspen Model	Difference
$\eta_{el\ SYST}$	19.5 ± 0.71 %	19.9 %	1.9 %
η_{TOT_SYST}	41.2 ± 5.3 %	37.7 %	8.6 %

3.3. Sensitivity analyses on the gasification system

Sensitivity analyses have been performed to evaluate the response of the model with respect to the changes of the operating conditions. In particular, the changes of the gasification temperature, equivalence ratio and moisture content of biomass on the gasification process have been considered in the following sections.

3.3.1. Effect of Equivalence Ratio

The amount of air entering the reactor is typically set in the range of ER= 0.20 – 0.50 in order to avoid complete combustion. Figure 9 shows the trend of the syngas molar compositions as a function of the ER. For low ER, H_2 and CO compositions increase, while CO_2 and CH_4 decrease; for higher values of ER, H_2 and CO decrease, CH_4 decreases until it reaches zero and CO_2 increases because the oxygen supply was increased. As the ER increases the production of CH_4 decreases due to because the reagents of the methanation reaction (C and H_2) were consumed in the oxidation reactions of hydrogen and carbon. An optimal value of ER, therefore, can be identified around 0.30.

Figure 9 shows the trend of syngas lower heating value LHV_{syngas} on ER. When ER increases, LHV_{syngas} decreases, due to the decrease of the amount of H_2, CO and CH_4 with ER. The higher oxidation rate of the fuel leads to a greater conversion in the syngas, with a consequent higher concentration of carbon dioxide and lower content of hydrocarbons, reducing LHV_{syngas}. On the other hand, for low ER values, biomass is not completely converted into volatiles and tar production is higher.

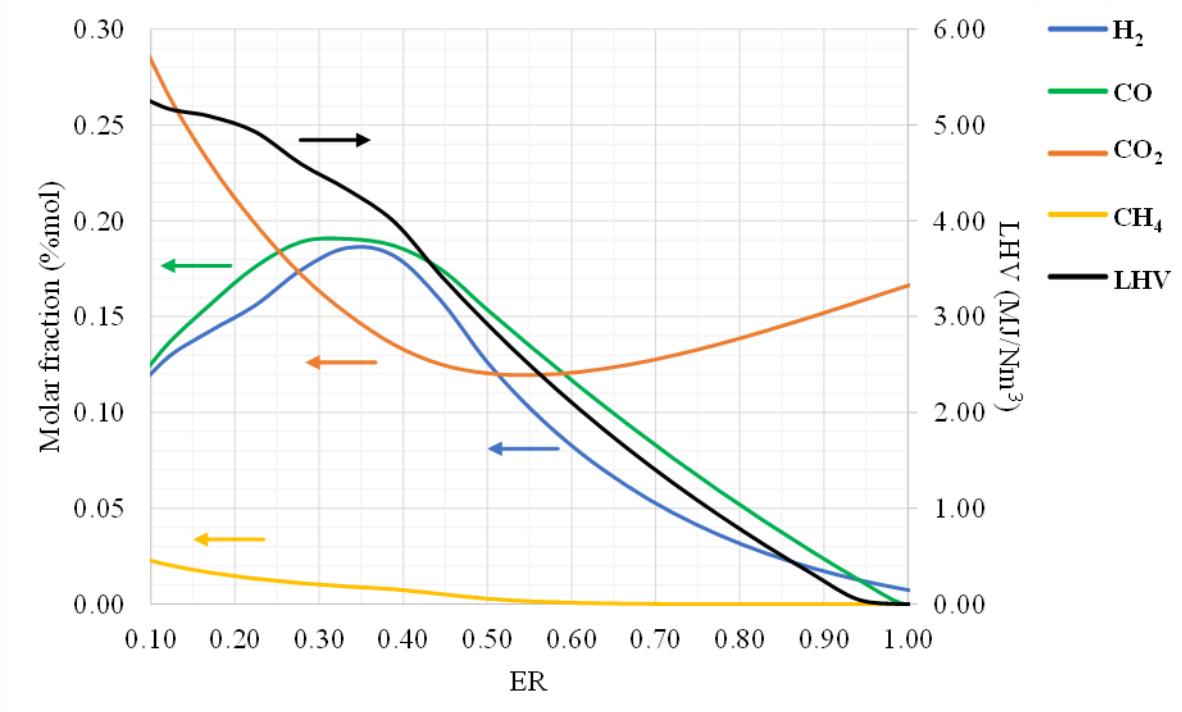

Figure 9 Effect of ER on the syngas molar composition and LHV.

3.3.2. *Effect of Gasification Temperature*

In the present work, the gasification temperature has been varied between 760 °C and 970°C. The gasification temperature affects the syngas molar composition, as shown in Figure 10, due to endothermic chemical reactions occurring inside the gasifier. Higher temperatures promote the products of endothermic reactions, according to the Le Chatelier Principle. A temperature increase implies a syngas production with a higher H_2 and CO content and, consequently, a higher LHV_{syngas}. On the other hand, however, the content of CH_4 and CO_2 follows the opposite trend. A temperature increase also implies that CH_4 decreases because the CH_4 formation reaction is exothermic.

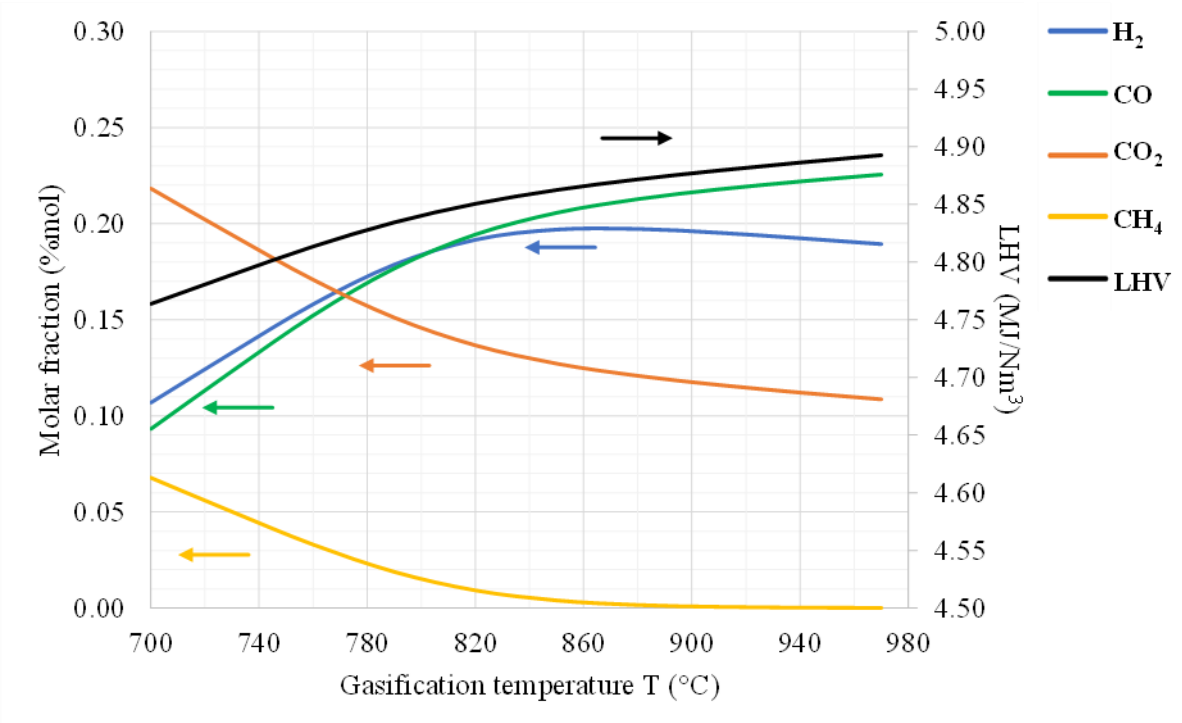

Figure 10. Effect of the gasification temperature on the syngas molar composition and LHV.

LHV_{syngas} increases with the gasification temperature, due to the significant influence of CO and H_2. The latter is slightly influenced by LHV of CH_4 since the CH_4 molar fraction decreases when the temperature gasification increases.

3.3.3. *Effect of Biomass Moisture*

MC has been varied from 5.00% to 40.0 % in order to investigate its influence on the syngas molar composition. Figure 11 shows the effect of the MC on the syngas molar composition. When MC increases, CO_2 content increases, while CO, H_2 and CH_4 contents decrease.
When MC increases from (Figure 12) LHV of syngas decreases, because more water is involved, more energy for gasification is necessary for the water evaporation, and consequently also the Electrical Power decreases.

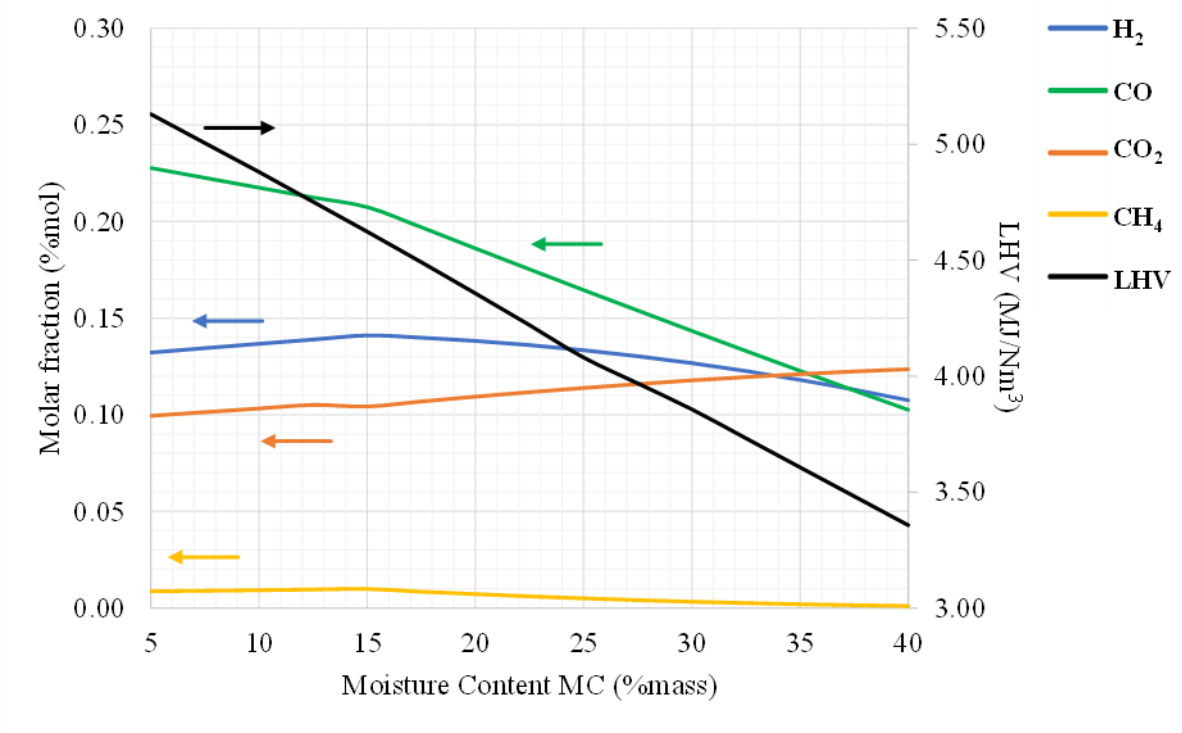

Figure 11 Effect of the MC on the syngas molar composition and LHV.

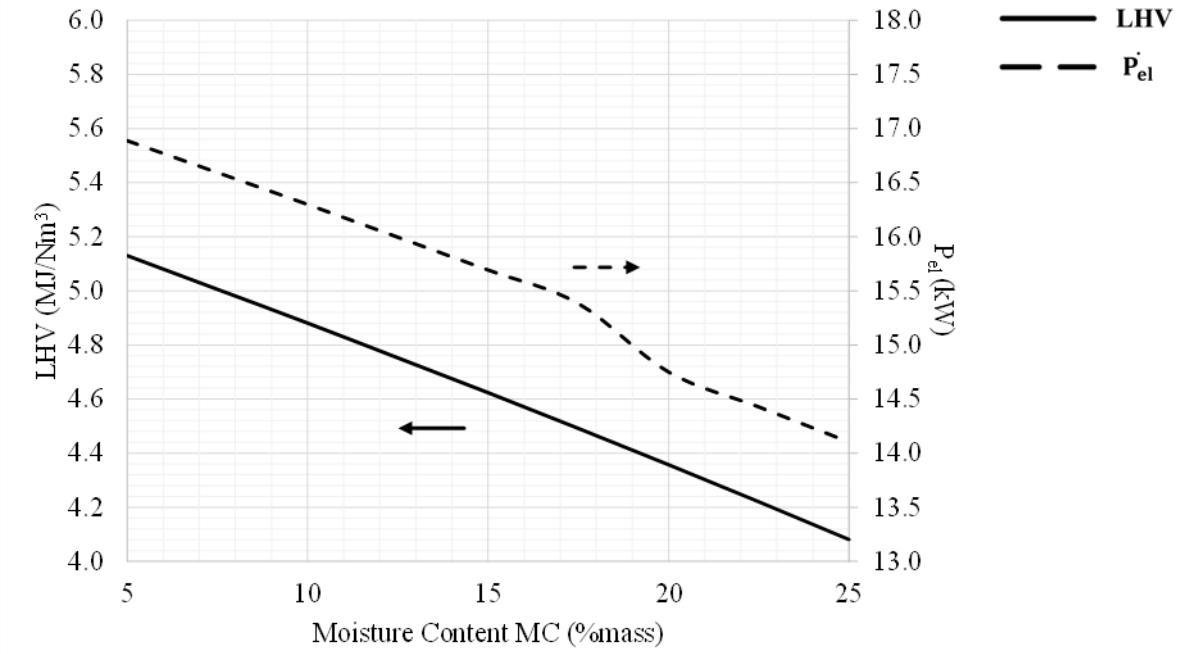

Figure 12 Effect of the MC on the Syngas lower heating value and the Electric Power of the ICE.

4. Conclusions

A simulation model of a real mCHP plant, based on a biomass gasifier coupled with an ICE, has been developed in Aspen Plus environment to predict the behaviour of the system. The

gasification model is based on the thermo-chemical equilibrium, minimizing the Gibbs free energy. The model reproduces the operation of the syngas cleaning unit, the ICE and the thermal recovery system. In particular, the thermal recovery system has been reproduced by implementing the detailed geometric features of the real heat exchangers of the mCHP with Aspen EDR environment.

An extensive experimental campaign has been carried out on the plant and the measured values have been associated with the corresponding expanded combined uncertainties. The model has been validated against the experimental data, and a good agreement has been observed, in particular for the syngas composition, the syngas LHV and the CGE.

Once assessed the predictiveness of the model, some parametric analyses have been carried out to improve the system performance, by analyzing the effects of the gasification temperature, the gasifier ER and the moisture content of biomass on the gasification process.

The parametric analyses of the gasification process have allowed to determine the optimal values of the main parameters. The main findings can be reported as follows:

- as regards the output energy fluxes, a net electric power of 16.3 kW and a total recovered thermal power of 14.6 kW have been calculated with the model, while the experimental values are 16.0 ± 0.60 kW and 17.8 ± 3.2 kW, respectively.
- the calculated values of the electrical and thermal efficiencies of the whole system are 19.9% and 17.8%, while the measured values are 19.5% ± 0.71 % and 21.7% ± 5.3 %, respectively.
- an increase of the gasification temperature above the operating condition of 800 °C may produce benefits regarding the LHV_{syngas}, which increases with a temperature increase.
- the ER has been varied from 0.10 to 1.00. The optimal value of the equivalence ratio has been found around 0.30, close to the real operative condition of ER (0.29).
- the effect of MC has also been considered and an optimal value of moisture content has been found around 10.0 %.

The present validated model has revealed to be a useful tool to analyze the performance of real mCHP plants. The future developments of the present work will include a detailed sensitivity analysis of the geometrical parameters in order to optimize the efficiencies of the whole system, such as the implementation of the model with different types of biomass.

Acknowledgments

The authors gratefully acknowledge the financial support of INNOVARE project, HORIZON2020 PON I&C 2014-2020 FESR, by the Italian Ministry of Economic Development (Ministero dello Sviluppo Economico - MISE), Grant n. 4700 of 20 November 2017. Moreover, the authors gratefully acknowledge Dr. Maria Vittoria Prati and Dr. Gabriele Di Blasio at the Istituto Motori of CNR for the analysis carried out on the syngas and on the engine, respectively, and Dr. Giovanna Ruoppolo and Dr. Massimo Urciuolo at the Combustion Research Institute of CNR for their valuable help in biomass characterization and experienced discussions.

Appendix A

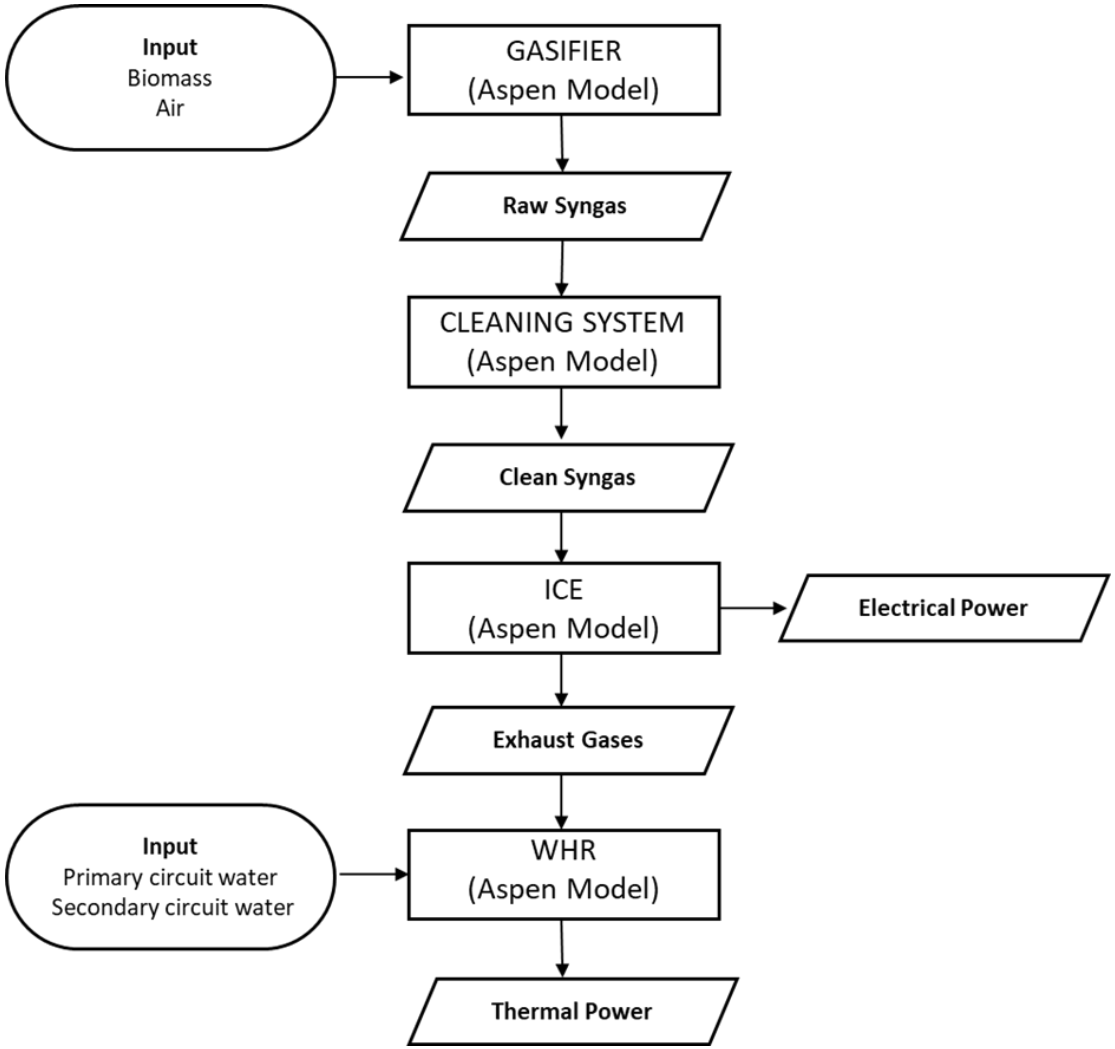

Figure A.1 Flow chart of the system.

Results of the experimental campaign

Table A.1 Temperature and mass flow rate values obtained during the experimental campaign, used to define the system efficiencies.

	BTDC	λ	T_{s1} [°C]	T_{s2} [°C]	T_{s3} [°C]	T_{ex2} [°C]	T_{ex3} [°C]	T_{p1} [°C]	T_{p2} [°C]	m_s [kg/s]	m_p [kg/s]
1	34	1.01	58.6 ±1.50	64.4 ±1.50	71.0 ±1.50	296.4 ±1.51	114.9 ±1.50	49.1 ±1.50	74.8 ±1.50	0.344 $\pm 1.99\times10^{-3}$	0.137 $\pm 1.19\times10^{-3}$
2	29	1.01	69.0 ±1.50	74.0 ±1.50	81.5 ±1.50	324.9 ±1.50	131.8 ±1.50	56.0 ±1.50	82.6 ±1.50	0.363 $\pm 2.10\times10^{-3}$	0.136 $\pm 1.12\times10^{-3}$
3	24	1.01	69.5 ±1.50	75.1 ±1.50	82.4 ±1.50	327.2 ±1.50	134.1 ±1.50	57.4 ±1.50	85.4 ±1.50	0.379 $\pm 2.19\times10^{-3}$	0.135 $\pm 1.21\times10^{-3}$
4	24	1.11	68.1 ±1.50	73.1 ±1.50	80.2 ±1.50	307.6 ±1.50	128.0 ±1.50	54.5 ±1.50	82.6 ±1.50	0.383 $\pm 2.21\times10^{-3}$	0.136 $\pm 1.18\times10^{-3}$
5	29	1.11	66.8 ±1.50	72.8 ±1.50	80.1 ±1.50	302.4 ±1.50	126.8 ±1.50	55.2 ±1.50	83.9 ±1.50	0.373 $\pm 2.15\times10^{-3}$	0.081 $\pm 5.30\times10^{-3}$
6	34	1.11	66.9 ±1.50	72.7 ±1.50	79.6 ±1.50	300.2 ±1.50	126.2 ±1.50	55.2 ±1.50	83.0 ±1.50	0.370 $\pm 2.14\times10^{-3}$	0.133 $\pm 1.08\times10^{-3}$
7	34	1.05	67.1 ±1.50	73.0 ±1.50	80.2 ±1.50	304.7 ±1.50	127.3 ±1.50	54.6 ±1.50	84.6 ±1.50	0.376 $\pm 2.17\times10^{-3}$	0.136 $\pm 1.10\times10^{-3}$
8	29	1.05	66.5 ±1.50	72.7 ±1.50	80.1 ±1.50	310.1 ±1.50	128.6 ±1.50	54.7 ±1.50	84.0 ±1.50	0.374 $\pm 2.16\times10^{-3}$	0.134 $\pm 1.19\times10^{-3}$
9	24	1.05	68.1 ±1.50	72.2 ±1.50	80.6 ±1.50	338.3 ±1.50	135.2 ±1.50	56.7 ±1.50	80.1 ±1.50	0.380 $\pm 2.19\times10^{-3}$	0.136 $\pm 1.11\times10^{-3}$
10	29	1.01	67.8 ±1.50	76.0 ±1.50	85.0 ±1.50	320.6 ±1.50	134.1 ±1.50	57.6 ±1.50	86.9 ±1.50	0.331 $\pm 1.91\times10^{-3}$	0.139 $\pm 1.22\times10^{-3}$
11	29	1.01	58.6 ±1.50	64.4 ±1.50	71.0 ±1.50	296.4 ±1.51	114.9 ±1.50	49.1 ±1.50	74.8 ±1.50	0.344 $\pm 1.99\times10^{-3}$	0.137 $\pm 1.19\times10^{-3}$

Table A.2 Electric and thermal powers used to define the system efficiencies.

	BTDC	λ	$\dot{P}_{el}$	Q_{PHE}	Q_{STHE}	Q_{TOT}
1	34	1.01	16.0 ±0.580	8.42 ±3.05	9.42 ±3.05	17.8 ±4.32
2	29	1.01	16.0 ±0.580	7.67 ±3.23	11.4 ±3.23	19.0 ±4.56
3	24	1.01	16.0 ±0.580	8.89 ±3.37	11.7 ±3.37	20.6 ±4.76
4	24	1.11	15.0 ±0.580	7.91 ±3.40	11.5 ±3.40	19.4 ±4.81
5	29	1.11	15.0 ±0.580	9.37 ±3.31	11.4 ±3.31	20.8 ±4.68
6	34	1.11	15.8 ±0.580	9.07 ±3.29	10.7 ±3.29	19.7 ±4.65
7	34	1.05	16.0 ±0.580	9.30 ±3.34	11.3 ±3.34	20.6 ±4.72
8	29	1.05	16.0 ±0.580	9.76 ±3.32	11.5 ±3.32	21.3 ±4.70
9	24	1.05	14.7 ±0.580	6.45 ±3.38	13.4 ±3.38	19.9 ±4.77
10	29	1.01	16.0 ±0.580	11.4 ±2.94	12.5 ±2.94	23.9 ±4.16
11	29	1.01	15.0 ±0.580	11.1 ±2.24	13.6 ±2.24	24.7 ±3.16

Table A.3 System efficiencies calculated by using the experimental results.

	BTDC	λ	$\eta_{el,ICE}$	$\eta_{th,ICE}$	$\eta_{TOT,ICE}$	$\eta_{el,ECO20}$	$\eta_{th,ECO20}$	$\eta_{TOT,ECO20}$
1	34	1.01	28.1% ±1.05%	31.3% ±7.58%	59.3% ±7.65%	19.5% ±0.710%	21.7% ±5.26%	41.2% ±5.31%
2	29	1.01	27.9% ±1.06%	33.2% ±7.97%	61.1% ±8.04%	19.5% ±0.710%	23.2% ±5.56%	42.7% ±5.61%
3	24	1.01	27.9% ±1.05%	35.9% ±8.31%	63.8% ±8.37%	19.5% ±0.710%	25.1% ±5.80%	44.6% ±5.85%
4	24	1.11	26.7% ±1.07%	34.4% ±8.56%	61.1% ±8.62%	18.3% ±0.710%	23.6% ±5.86%	41.9% ±5.90%
5	29	1.11	26.8% ±1.07%	37.0% ±8.36%	63.8% ±8.43%	18.0% ±0.690%	24.9% ±5.62%	42.9% ±5.66%
6	34	1.11	28.4% ±1.08%	35.5% ±8.36%	63.9% ±8.43%	19.0% ±0.700%	23.7% ±5.58%	42.7% ±5.63%
7	34	1.05	28.1% ±1.06%	36.1% ±8.30%	64.2% ±8.37%	19.2% ±0.690%	24.7% ±5.67%	43.9% ±5.71%
8	29	1.05	28.2% ±1.06%	37.5% ±8.29%	65.7% ±8.36%	19.2% ±0.690%	25.6% ±5.64%	44.8% ±5.69%
9	24	1.05	25.9% ±1.06%	35.0% ±8.42%	60.9% ±8.49%	17.6% ±0.700%	23.8% ±5.73%	41.5% ±5.77%
10	29	1.01	27.6% ±1.05%	41.3% ±7.20%	68.9% ±7.28%	19.2% ±0.690%	28.7% ±5.00%	47.9% ±5.05%
11	29	1.01	25.7% ±1.03%	42.2% ±5.44%	67.9% ±5.53%	19.3% ±0.740%	31.7% ±4.06%	51.0% ±4.13%

References

[1] "2030 Climate and Energy Framework Climate Action." [Online]. Available: https://ec.europa.eu/clima/policies/strategies/2030_en.

[2] R. Passey, T. Spooner, I. MacGill, M. Watt, and K. Syngellakis, "The potential impacts of grid-connected distributed generation and how to address them: A review of technical and non-technical factors," *Energy Policy*, vol. 39, no. 10, pp. 6280–6290, Oct. 2011.

[3] A. Demirbas, "Biofuels sources, biofuel policy, biofuel economy and global biofuel projections," *Energy Convers. Manag.*, vol. 49, no. 8, pp. 2106–2116, Aug. 2008.

[4] L. Dong, H. Liu, and S. Riffat, "Development of Small-Scale and Micro-Scale Biomass-Fuelled CHP Systems-A literature review."

[5] V. Dhyani and T. Bhaskar, "A comprehensive review on the pyrolysis of lignocellulosic biomass," *Renew. Energy*, vol. 129, pp. 695–716, Dec. 2018.

[6] Q. Xiong, S. C. Kong, and A. Passalacqua, "Development of a generalized numerical framework for simulating biomass fast pyrolysis in fluidized-bed reactors," *Chem. Eng. Sci.*, vol. 99, pp. 305–313, Aug. 2013.

[7] J. J. Hernández, G. Aranda-Almansa, and A. Bula, "Gasification of biomass wastes in an entrained flow gasifier: Effect of the particle size and the residence time," *Fuel Process. Technol.*, vol. 91, no. 6, pp. 681–692, Jun. 2010.

[8] S. Chopra and A. K. Jain, "A Review of Fixed Bed Gasification Systems for Biomass," *Agric. Eng. Int. CIGR J.*, Apr. 2007.

[9] J. A. Ruiz, M. C. Juárez, M. P. Morales, P. Muñoz, and M. A. Mendívil, "Biomass gasification for electricity generation: Review of current technology barriers," *Renew. Sustain. Energy Rev.*, vol. 18, pp. 174–183, Feb. 2013.

[10] C. Gai and Y. Dong, "Experimental study on non-woody biomass gasification in a downdraft gasifier," *Int. J. Hydrogen Energy*, vol. 37, no. 6, pp. 4935–4944, Mar. 2012.

[11] C. Di Blasi, G. Signorelli, and G. Portoricco, "Countercurrent fixed-bed gasification of biomass at laboratory scale," *Ind. Eng. Chem. Res.*, vol. 38, no. 7, pp. 2571–2581, 1999.

[12] Z. A. Zainal, A. Rifau, G. A. Quadir, and K. N. Seetharamu, "Experimental investigation of a downdraft biomass gasifier," *Biomass and Bioenergy*, vol. 23, no. 4, pp. 283–289, 2002.

[13] M. Dogru, C. R. Howarth, G. Akay, B. Keskinler, and A. A. Malik, "Gasification of hazelnut shells in a downdraft gasifier," *Energy*, vol. 27, no. 5, pp. 415–427, 2002.

[14] T. H. Jayah, L. Aye, R. J. Fuller, and D. F. Stewart, "Computer simulation of a downdraft wood gasifier for tea drying," *Biomass and Bioenergy*, vol. 25, no. 4, pp. 459–469, 2003.

[15] T. Hanaoka, S. Inoue, S. Uno, T. Ogi, and T. Minowa, "Effect of woody biomass components on air-steam gasification," *Biomass and Bioenergy*, vol. 28, no. 1, pp. 69–76, 2005.

[16] P. N. Sheth and B. V. Babu, "Experimental studies on producer gas generation from wood waste in a downdraft biomass gasifier," *Bioresour. Technol.*, vol. 100, no. 12, pp. 3127–3133, 2009.

[17] A. K. Sharma, "Experimental study on 75 kWth downdraft (biomass) gasifier system," *Renew. Energy*, vol. 34, no. 7, pp. 1726–1733, 2009.

[18] J. D. Martínez, E. E. Silva Lora, R. V. Andrade, and R. L. Jaén, "Experimental study on biomass gasification in a double air stage downdraft reactor," *Biomass and Bioenergy*, vol. 35, no. 8, pp. 3465–3480, 2011.

[19] Z. A. Zainal, R. Ali, C. H. Lean, and K. N. Seetharamu, "Prediction of performance of a downdraft gasifier using equilibrium modeling for different biomass materials," *Energy Convers. Manag.*, vol. 42, no. 12, pp. 1499–1515, 2001.

[20] S. Jarungthammachote and A. Dutta, “Thermodynamic equilibrium model and second law analysis of a downdraft waste gasifier,” *Energy*, vol. 32, no. 9, pp. 1660–1669, 2007.
[21] A. K. Sharma, “Equilibrium modeling of global reduction reactions for a downdraft (biomass) gasifier,” *Energy Convers. Manag.*, vol. 49, no. 4, pp. 832–842, 2008.
[22] M. Vaezi, M. Passandideh-Fard, M. Moghiman, and M. Charmchi, “Modeling biomass gasification: A new approach to utilize renewable sources of energy,” in *ASME International Mechanical Engineering Congress and Exposition, Proceedings*, 2009, vol. 8, pp. 927–935.
[23] N. S. Barman, S. Ghosh, and S. De, “Gasification of biomass in a fixed bed downdraft gasifier - A realistic model including tar,” *Bioresour. Technol.*, vol. 107, pp. 505–511, Mar. 2012.
[24] V. B. Silva and A. Rouboa, “Using a two-stage equilibrium model to simulate oxygen air enriched gasification of pine biomass residues,” *Fuel Process. Technol.*, vol. 109, pp. 111–117, 2013.
[25] M. Costa, L. Villetta, and N. Massarotti, “Optimal Tuning of a Thermo-Chemical Equilibrium Model for Downdraft Biomass Gasifiers,” in *CHEMICAL ENGINEERING TRANSACTIONS*, 2015, vol. 43.
[26] C. Di Blasi, “Dynamic behaviour of stratified downdraft gasifiers,” in *Chemical Engineering Science*, 2000, vol. 55, no. 15, pp. 2931–2944.
[27] D. L. Giltrap, R. McKibbin, and G. R. G. Barnes, “A steady state model of gas-char reactions in a downdraft biomass gasifier,” *Sol. Energy*, vol. 74, no. 1, pp. 85–91, 2003.
[28] E. D. Gordillo and A. Belghit, “A downdraft high temperature steam-only solar gasifier of biomass char: A modelling study,” *Biomass and Bioenergy*, vol. 35, no. 5, pp. 2034–2043, May 2011.
[29] F. V. Tinaut, A. Melgar, J. F. Pérez, and A. Horrillo, “Effect of biomass particle size and air superficial velocity on the gasification process in a downdraft fixed bed gasifier. An experimental and modelling study,” *Fuel Process. Technol.*, vol. 89, no. 11, pp. 1076–1089, Nov. 2008.
[30] A. K. Sharma, “Modeling and simulation of a downdraft biomass gasifier 1. Model development and validation,” *Energy Convers. Manag.*, vol. 52, no. 2, pp. 1386–1396, Feb. 2011.
[31] M. Simone, C. Nicolella, and L. Tognotti, “Numerical and experimental investigation of downdraft gasification of woody residues,” *Bioresour. Technol.*, vol. 133, pp. 92–101, 2013.
[32] X. Gao, Y. Zhang, B. Li, and X. Yu, “Model development for biomass gasification in an entrained flow gasifier using intrinsic reaction rate submodel,” *Energy Convers. Manag.*, vol. 108, pp. 120–131, 2016.
[33] T. Jakobs, N. Djordjevic, S. Fleck, M. Mancini, R. Weber, and T. Kolb, “Gasification of high viscous slurry R&D on atomization and numerical simulation,” *Appl. Energy*, vol. 93, pp. 449–456, 2012.
[34] I. Janajreh and M. Al Shrah, “Numerical and experimental investigation of downdraft gasification of wood chips,” *Energy Convers. Manag.*, vol. 65, pp. 783–792, 2013.
[35] M. Puig-Arnavat, J. A. Hernández, J. C. Bruno, and A. Coronas, “Artificial neural network models for biomass gasification in fluidized bed gasifiers,” *Biomass and Bioenergy*, vol. 49, pp. 279–289, 2013.
[36] Y. Li, L. Yan, B. Yang, W. Gao, and M. R. Farahani, “Simulation of biomass gasification in a fluidized bed by artificial neural network (ANN),” *Energy Sources, Part A Recover. Util. Environ. Eff.*, vol. 40, no. 5, pp. 544–548, 2018.
[37] G. Xiao *et al.*, “Gasification characteristics of MSW and an ANN prediction model,” *Waste Manag.*, vol. 29, no. 1, pp. 240–244, 2009.

[38] K. G. Mansaray, A. M. Al-Taweel, A. E. Ghaly, F. Hamdullahpur, and V. I. Ugursal, "Mathematical modeling of a fluidized bed rice husk gasifier: Part I - model development," *Energy Sources*, vol. 22, no. 1, pp. 83–98, 2000.
[39] N. Ramzan, A. Ashraf, S. Naveed, and A. Malik, "Simulation of hybrid biomass gasification using Aspen plus: A comparative performance analysis for food, municipal solid and poultry waste," *Biomass and Bioenergy*, vol. 35, no. 9, pp. 3962–3969, 2011.
[40] P. C. Kuo, W. Wu, and W. H. Chen, "Gasification performances of raw and torrefied biomass in a downdraft fixed bed gasifier using thermodynamic analysis," *Fuel*, vol. 117, no. PARTB, pp. 1231–1241, 2014.
[41] H. Gu, Y. Tang, J. Yao, and F. Chen, "Study on biomass gasification under various operating conditions," *J. Energy Inst.*, vol. 92, no. 5, pp. 1329–1336, Oct. 2019.
[42] R. Tavares, E. Monteiro, F. Tabet, and A. Rouboa, "Numerical investigation of optimum operating conditions for syngas and hydrogen production from biomass gasification using Aspen Plus," *Renew. Energy*, vol. 146, pp. 1309–1314, Feb. 2020.
[43] "Biomass Magazine - The Latest News on Biomass Power, Fuels and Chemical." .
[44] "Masera, D., Faaji A. Renewable Energy for Inclusive and Sustainable Development. The Case of Biomass Gasification. UNIDO, 2014."
[45] A. A. C. M. Beenackers, "Biomass gasification in moving beds, a review of European technologies," *Renewable Energy*, vol. 16, no. 1–4. Pergamon, pp. 1180–1186, 1999.
[46] J. Ahrenfeldt, T. P. Thomsen, U. Henriksen, and L. R. Clausen, "Biomass gasification cogeneration – A review of state of the art technology and near future perspectives," *Appl. Therm. Eng.*, vol. 50, no. 2, pp. 1407–1417, 2013.
[47] D. Mertzis, P. Mitsakis, S. Tsiakmakis, P. Manara, A. Zabaniotou, and Z. Samaras, "Performance analysis of a small-scale combined heat and power system using agricultural biomass residues: The SMARt-CHP demonstration project," *Energy*, vol. 64, pp. 367–374, 2014.
[48] D. Barisano, "Biomass Gasification for Energy Purposes Country Report - Italy."
[49] M. Baratieri, P. Baggio, B. Bosio, M. Grigiante, and G. A. Longo, "The use of biomass syngas in IC engines and CCGT plants: A comparative analysis," *Appl. Therm. Eng.*, vol. 29, no. 16, pp. 3309–3318, 2009.
[50] M. Trninic *et al.*, "Mathematical modelling and performance analysis of a small-scale combined heat and power system based on biomass waste downdraft gasification," in *Lecture Notes in Networks and Systems*, vol. 54, 2019, pp. 159–173.
[51] A. Inayat, M. Ahmad, M. Mutalib, S. Y.-C. Engineering, and undefined 2011, "Heat integration analysis of gasification process for hydrogen production from oil palm empty fruit bunch," *academia.edu*.
[52] M. Villarini, V. Marcantonio, A. Colantoni, and E. Bocci, "Sensitivity Analysis of Different Parameters on the Performance of a CHP Internal Combustion Engine System Fed by a Biomass Waste Gasifier," *Energies*, vol. 12, no. 4, p. 688, 2019.
[53] A. M. L. Násner *et al.*, "Refuse Derived Fuel (RDF) production and gasification in a pilot plant integrated with an Otto cycle ICE through Aspen Plus™ modelling: Thermodynamic and economic viability," *Waste Management*, vol. 69. Elsevier Ltd, pp. 187–201, 2017.
[54] M. Formica, S. Frigo, and R. Gabbrielli, "Development of a new steady state zero-dimensional simulation model for woody biomass gasification in a full scale plant," *Energy Convers. Manag.*, vol. 120, pp. 358–369, 2016.
[55] F. Emun, M. Gadalla, T. Majozi, and D. Boer, "Integrated gasification combined cycle (IGCC) process simulation and optimization," *Comput. Chem. Eng.*, vol. 34, no. 3, pp. 331–338, 2010.
[56] V. Madzivhandila, T. Majozi, and T. Zhelev, "Process integration as an optimization tool

in clean coal technology: A focus on IGCC.," *Chem. Eng. Trans.*, vol. 18, pp. 941–946, 2009.
[57] W. Lan, G. Chen, X. Zhu, X. Wang, C. Liu, and B. Xu, "Biomass gasification-gas turbine combustion for power generation system model based on ASPEN PLUS," *Sci. Total Environ.*, vol. 628–629, pp. 1278–1286, Jul. 2018.
[58] "Aspen Plus | Leading Process Simulation Software | AspenTech." [Online]. Available: https://www.aspentech.com/en/products/engineering/aspen-plus.
[59] W. Gumz, *Gas Producers and Blast Furnaces: Theory and Methods of Calculation*. John Wiley & Sons, 1950.
[60] J. M. de Andrés, M. Vedrenne, M. Brambilla, and E. Rodríguez, "Modeling and model performance evaluation of sewage sludge gasification in fluidized-bed gasifiers using Aspen Plus," *J. Air Waste Manag. Assoc.*, vol. 69, no. 1, pp. 23–33, 2019.
[61] S. A. Channiwala and P. P. Parikh, "A unified correlation for estimating HHV of solid, liquid and gaseous fuels," *Fuel*, vol. 81, no. 8, pp. 1051–1063, May 2002.
[62] "Phyllis2 - Database for the physico-chemical composition of biomass." .
[63] F. Arpino, N. Massarotti, A. Mauro, and L. Vanoli, "Metrological analysis of the measurement system for a micro-cogenerative SOFC module," *Int. J. Hydrogen Energy*, vol. 36, no. 16, pp. 10228–10234, Aug. 2011.
[64] "ISO - ISO/IEC Guide 98-3:2008 - Uncertainty of measurement — Part 3: Guide to the expression of uncertainty in measurement (GUM:1995)." .